



Cite this: DOI: 10.1039/d3ja00440f

In situ Sr–Nd isotope analysis of vesuvianite by LA-MC-ICP-MS: methodology and application†

 Qin-Di Wei,^{ab} Yue-Heng Yang,^{ab} Hao Wang,^{ab} Shi-Tou Wu,^{ab} Ming Yang,^c Chao Huang,^{ab} Lei Xu,^{ab} Lie-Wen Xie,^{ab} Jin-Hui Yang^{ab} and Fu-Yuan Wu^{ab}

Vesuvianite is a common accessory mineral that usually occurs in metamorphosed and metasomatised, argillaceous carbonate rocks (*i.e.*, skarn rocks) and as a late crystallising phase in igneous rocks such as nepheline syenites. Vesuvianite is a Ca-rich mineral that preferentially incorporates Sr and light rare earth elements (LREEs). Given that vesuvianite is susceptible to alteration and commonly contains inclusions, *in situ* laser ablation analysis is the preferred approach for measuring its Sr–Nd isotopic compositions. The use of matrix-matched and homogeneous reference materials is a prerequisite for laser ablation isotope analyses. Two in-house vesuvianite standards M6635 and M659 were used for external correction during *in situ* laser ablation analysis for Sr and Nd isotopic compositions, respectively. In this paper, we apply *in situ* Sr and Sm–Nd isotope analyses for 11 vesuvianite samples (M6635, M784, M1377, M660, M1439, M1450, M6601, 13MDL176, Wilui, Hazlov, and Goodall) from different locations. The obtained Sr and Sm–Nd isotopic compositions for these vesuvianite samples are consistent with those obtained by solution-based methods using MC-ICP-MS, which demonstrates the robustness of our analytical methods. We recommend that samples M6635, M784, M1377, and M1450 are suitable vesuvianite reference materials for *in situ* Sr isotope analyses, and sample M659 is a potential vesuvianite reference material for *in situ* Sm–Nd isotope analyses.

 Received 11th December 2023
 Accepted 20th March 2024

DOI: 10.1039/d3ja00440f

rsc.li/jaas

1. Introduction

Vesuvianite, $(\text{Ca},\text{Na})_{19}(\text{Al},\text{Mg},\text{Fe})_{13}(\text{SiO}_4)_{10}(\text{Si}_2\text{O}_7)_4(\text{OH},\text{F},\text{O})_{10}$, usually occurs in relatively low-pressure rocks, such as skarn ore deposits, metamorphosed and metasomatised argillaceous carbonate rocks,^{1–3} and as a late phase in igneous rocks (*e.g.*, nepheline syenites).⁴ It can also be found in high-pressure metamorphic jadeitite.⁵ Despite this wide range of occurrences, vesuvianite remains one of the least well understood of all rock-forming minerals owing to its complex crystal structure and wide range of possible substitutions, which make it difficult to constrain metamorphic reactions and thermodynamic models.^{2,6} However, these complexities make it possible to constrain the formation environment of vesuvianite and the geochemistry of the fluid or melt from which it crystallised.^{6–9} Vesuvianite can also act as a geothermometer owing to the sensitivity of its symmetry to the crystallisation temperature.¹⁰

The high isomorphous capacity and stability of vesuvianite favours the incorporation of variable amounts of U (several tens or hundreds of $\mu\text{g g}^{-1}$), making it a potential mineral for U–Pb dating.^{11–14} As a Ca-rich mineral, vesuvianite has moderate or high Sr (several tens to thousands of $\mu\text{g g}^{-1}$) and low Rb ($<1 \mu\text{g g}^{-1}$) contents,^{6,7,9} which mean the measured $^{87}\text{Sr}/^{86}\text{Sr}$ ratio represents the initial Sr isotopic composition of the fluid or melt from which the vesuvianite crystallised.^{15,16} Furthermore, vesuvianite can be enriched in light rare earth elements (LREEs).^{6,7,9} Linking accessory mineral U–Pb ages with Sm–Nd isotopic data, such as for apatite, titanite, monazite, bastnäsite, and allanite,^{16–20} can provide important insights into the origins and evolution of magmas, fluids, and metamorphism. Therefore, vesuvianite has the potential to provide important petrogenetic and hydrothermal information.

Strontium or Nd isotopic data can be obtained using conventional multi-collector thermal ionisation mass spectrometry (TIMS), which is the benchmark method for Sr–Nd isotope analysis due to its high precision. Ma *et al.*²¹ reported a TIMS Sm–Nd isochron age of 141 ± 11 Ma for skarn-type minerals, including vesuvianite and garnet, from the Dongpo ore field, Nanling Range, South China. Gilg *et al.*²² presented mineral chemical, fluid inclusion, and radiogenic (Sr, Nd, and Pb) and stable (C and O) isotope data for skarns and associated cognate and xenolithic nodules from the Mt. Somma–Vesuvius

^aState Key Laboratory of Lithospheric Evolution, Institute of Geology and Geophysics, Chinese Academy of Sciences, Beijing 100029, China. E-mail: yangyueheng@mail.iggcas.ac.cn

^bCollege of Earth and Planetary Science, University of Chinese Academy of Sciences, Beijing 100049, China

^cHainan Institute of Zhejiang University, Sanya 572025, China

† Electronic supplementary information (ESI) available. See DOI: <https://doi.org/10.1039/d3ja00440f>

volcanic complex, Italy. They obtained the $^{143}\text{Nd}/^{144}\text{Nd}$ ratios of two vesuvianite samples using the TIMS method. The Nd isotopic compositions of vesuvianite, wollastonite, and whole rocks suggested that substantial crustal contamination had occurred in the skarns.

Bulk analysis of single crystals is more difficult and time-consuming than *in situ* microbeam methods, such as laser ablation multiple-collector inductively coupled plasma mass spectrometry (LA-MC-ICP-MS) and secondary ion mass spectrometry (SIMS).¹⁶ However, due to the low sample consumption and the isobaric interference of ^{87}Rb on ^{87}Sr during SIMS analysis, precision cannot be guaranteed and measurement is more time-consuming than the LA-MC-ICP-MS method, especially for low Sr ($<500\ \mu\text{g g}^{-1}$) samples.^{23,24} Given that vesuvianite is susceptible to alteration and commonly contains inclusions, *in situ* laser ablation analysis is considered to be the most suitable analytical method and can record detailed geological information regarding melt sources and metamorphic events (*e.g.*, ref. 25 and 26). However, no well-characterised vesuvianite reference material is available for *in situ* Sr–Nd isotope analyses. A key component of *in situ* isotope analyses by LA-MC-ICP-MS is monitoring and correcting for plasma- and laser-induced elemental fractionation, particularly for Sm–Nd isotope measurements, because $^{147}\text{Sm}/^{144}\text{Nd}$ fractionation and the isobaric interference of ^{144}Sm on ^{144}Nd are analytical issues during laser ablation analysis.^{15,27–30} The effects of non-matrix matching on the fractionation between ^{147}Sm and ^{144}Nd remains controversial.^{17,25,30} In terms of Sr isotope analysis, the sample-standard bracketing method is often used to correct for possible instrumental mass-independent fractionation effects.^{31,32} Therefore, using a matrix-matched and homogeneous reference material is a prerequisite for calibration during analytical sessions.

In this paper, we develop the first Sr–Nd isotope analyses of vesuvianite crystals obtained using both solution- and laser ablation-based techniques and data for a suite of well-characterised vesuvianite samples for use as reference materials in *in situ* Sr–Nd isotope studies. Moreover, seven applications including eleven samples were further exemplified.

2. Analytical methods

All vesuvianite samples were mounted in epoxy resin blocks and polished to expose the crystal interiors prior to analysis. Samples for solution Sr and Sm–Nd isotope analyses were analysed *via* MC-ICP-MS. The *in situ* trace element analyses obtained *via* LA-ICP-MS and the Sr–Nd isotopic measurements obtained by LA-MC-ICP-MS were undertaken at the State Key Laboratory of Lithospheric Evolution (SKLLE), Institute of Geology and Geophysics (IGG), Chinese Academy of Sciences (CAS), Beijing, China.

2.1 *In situ* trace element analysis

An Agilent 7500a Q-ICP-MS instrument coupled to a 193 nm ArF excimer LA system was used to determine trace element contents. Prior to analysis, the pulse/analogue (P/A) factor of the detector was calibrated using a standard tuning solution. Helium was used as the carrier gas through the ablation cell and

mixed with Ar downstream of the ablation cell. During LA, the instrument was optimised using the NIST SRM 610 glass reference material. The carrier and make-up gas flows were optimised to obtain a stable maximum signal intensity for $^{238}\text{U}^+$ while keeping the ThO^+/Th^+ ratio to $<0.5\%$ and Th/U to ~ 1 .

The detailed parameter settings are presented in Table 1. A laser fluence of $\sim 5\ \text{J cm}^{-2}$, a spot size of $60\ \mu\text{m}$, and a repetition rate of 5 Hz were used. All LA-ICP-MS measurements were carried out using time-resolved analysis in fast, peak jumping mode. The dwell time for each isotope was set to 6 ms for ^7Li , ^{11}B , ^{75}As , ^{85}Rb , ^{88}Sr , ^{89}Y , ^{90}Zr , ^{178}Hf , and REEs; 10 ms for ^{232}Th and ^{238}U ; 15 ms for ^{204}Pb , ^{206}Pb , and ^{208}Pb ; and 30 ms for ^{207}Pb . Each spot analysis consisted of 30 s of background and 60 s of sample data acquisition. Quantitative trace element results were obtained *via* calibration of relative element sensitivities using NIST SRM 610 (ref. 33) as the primary reference material, and ARM-1 (ref. 34 and 35) was analysed to assess data quality. Each analysis was also normalised to Si as an internal standard (SiO_2 contents were measured previously by EPMA). Data were processed using Glitter software.³⁶

2.2 *In situ* Sr and Sm–Nd isotope analysis

A Thermo Scientific Neptune Plus MC-ICP-MS coupled to a 193 nm ArF excimer LA system was used to determine Sr and Sm–Nd isotopic compositions. The laser fluence was set to $\sim 6\ \text{J cm}^{-2}$. A laser spot size of $60\text{--}160\ \mu\text{m}$ was employed with a $6\text{--}8\ \text{Hz}$ repetition rate, depending on the Sr and Nd concentrations of the samples. We used Jet sample and X skimmer cones in combination with the addition of $4\ \text{mL min}^{-1}\ \text{N}_2$ to improve the signal intensity during *in situ* Sr and Sm–Nd isotope measurements.³⁷ Detailed instrumental and measurement conditions are presented in Table 1. Prior to analysis, the instrument was tuned using a standard solution to obtain maximum sensitivity. The Sr isotope measurements consisted of 1 block of 200 cycles with an integration time of 0.524 s, while the data acquisition of Sm–Nd isotope involved one block of 200 cycles with an integration time of 0.262 s per cycle. Each spot analysis consisted of 25 s of measurement of the Ar–Kr gas blank with the laser off, followed by 75 s of Sr isotope data acquisition during LA. For *in situ* Sm–Nd isotope analysis, each spot analysis consisted of 60 s sample data acquisition.^{18,20,29,38} A well-characterised reference material is essential for microanalysis. As discussed below, M6635 vesuvianite has a nearly uniform Sr isotopic composition and can be used as an external standard. M659 vesuvianite was also used as an external standard for the other vesuvianite samples during the Sm–Nd isotope measurements. Meanwhile, we used the Slyudyanka apatite ($^{87}\text{Sr}/^{86}\text{Sr} = 0.70768 \pm 0.00003$)¹⁶ and NIST SRM 610 ($^{143}\text{Nd}/^{144}\text{Nd} = 0.511927$)³⁹ for data quality control during the analyses. Every 10 sample analyses were followed by 2 Slyudyanka apatite or NIST SRM 610 analyses. During the period of data acquisition, Slyudyanka apatite gave 0.70778 ± 0.00009 (2s; $n = 87$) for $^{87}\text{Sr}/^{86}\text{Sr}$ and NIST SRM 610 gave 0.511914 ± 0.000047 (2s; $n = 56$) for $^{143}\text{Nd}/^{144}\text{Nd}$.

To obtain accurate $^{87}\text{Sr}/^{86}\text{Sr}$ ratios by LA-MC-ICP-MS, the contribution from the isobaric interferences of Kr, Yb^{2+} , Er^{2+} , and Rb must be carefully corrected.^{15,16,19,40,41} Data reduction was

Table 1 Typical instrumental parameters for trace element and Sr–Nd isotope analysis of the vesuvianite samples

Laser ablation systems		Coherent geolas HD								
Laser system	ComPex 102, ArF excimer UV 193 nm									
Ablation cell and volume	Standard circle low volume cell, volume <i>ca.</i> 4 cm ³									
Fluence	~ 5 J cm ⁻² for trace element analysis, ~ 6 J cm ⁻² for Sr–Nd isotope analysis									
Repetition rate	5–8 Hz									
Spot diameter nominal	60 μm for trace element analysis, 60–160 μm for Sr isotope analysis, 120 μm for Sm–Nd isotope analysis									
Ablation duration	60 s for trace elements, 75 s for Sr isotope, 60 s for Sm–Nd isotope									
Sampling mode	Static spot ablation									
Sample preparation	Conventional mineral separation, 1 inch resin mount									
Mass spectrometers		Thermo fisher neptune MC-ICP-MS				Agilent 7500a Q-ICP-MS				
RF forward power (W)	~1200					RF forward power (W)	~1350			
Cool gas (L min ⁻¹)	16					Carrier gas (L min ⁻¹)	~1.1			
Auxiliary gas (L min ⁻¹)	0.8					Sample depth (mm)	~4.5			
Carrier gas flow (L min ⁻¹)	~1.1					Interface cone	Ni			
N ₂ gas flow (mL min ⁻¹)	4					Dwell times	15 ms for ²⁰⁴ Pb, ²⁰⁶ Pb and ²⁰⁸ Pb, 30 ms for ²⁰⁷ Pb, 10 ms for ²³² Th and ²³⁸ U, 6 ms for other elements			
Sampling cone	Jet cone					Analysis duration	90 s (including 30 s background, 60 s ablation)			
Skimmer cone	X cone									
Sampling mode	9 blocks of 10 cycles for Sr, Nd (solution) 1 block of 40 cycles for Sm (solution) 1 block of 200 cycles (laser)									
Intergration time	4 s for Nd (solution), 2 s for Sm (solution) 0.524 s for Sr (laser), 0.262 s for Sm–Nd (laser)									
Background/baseline	30s on peak zero (OPZ)									
MC-ICP-MS cup configuration										
Faraday cups	L4	L3	L2	L1	Center	H1	H2	H3	H4	
Nominal mass	83	83.5	84	85	86	86.5	87	88	89	
Sr ⁺			⁸⁴ Sr ⁺		⁸⁶ Sr ⁺		⁸⁷ Sr ⁺	⁸⁸ Sr ⁺		
[Kr ⁺ , Rb ⁺ , HREE ²⁺]	⁸³ Kr ⁺ , ¹⁶⁶ Er ²⁺	¹⁶⁷ Er ²⁺	⁸⁴ Kr ⁺ , ¹⁶⁸ Er ²⁺ , ¹⁶⁸ Yb ²⁺	⁸⁵ Rb ⁺ , ¹⁷⁰ Er ²⁺ , ¹⁷⁰ Yb ²⁺	⁸⁶ Kr ⁺ , ¹⁷² Yb ²⁺	¹⁷³ Yb ²⁺	⁸⁷ Rb ⁺ , ¹⁷⁴ Yb ²⁺	¹⁷⁶ Yb ²⁺	⁸⁹ Y ⁺	
Nominal mass	142	143	144	145	146	147	148	149	150	
Nd ⁺	¹⁴² Nd ⁺	¹⁴³ Nd ⁺	¹⁴⁴ Nd ⁺	¹⁴⁵ Nd ⁺	¹⁴⁶ Nd ⁺		¹⁴⁸ Nd ⁺		¹⁵⁰ Nd ⁺	
[Ce ⁺ , Sm ⁺]	¹⁴² Ce ⁺		¹⁴⁴ Sm ⁺			¹⁴⁷ Sm ⁺	¹⁴⁸ Sm ⁺	¹⁴⁹ Sm ⁺	¹⁵⁰ Sm ⁺	
Data processing										
Gas blank	30 s on peak zero subtracted									
Calibration strategy	NIST 610 used as external standard and ²⁹ Si used as internal standard for calibration of trace element content; M6635 used as Sr isotope reference material; M659 used as Sm–Nd isotope reference material									
Data processing package	For trace elements, Glitter software was used for elemental fractionation, instrumental mass bias calibration, uncertainty propagation. For Sr–Nd isotope, an in-house Microsoft Excel macro written in VBA (visual basic for applications) was used for Sr and Nd isotope mass fraction correction, interference correction and uncertainty propagation									
Uncertainty level	All results are quoted with 2 sigma absolute uncertainty unless otherwise stated									

conducted offline using an in-house Excel macro. The interferences of ⁸⁴Kr and ⁸⁶Kr on ⁸⁴Sr and ⁸⁶Sr, respectively, were removed using the Ar–Kr gas blank measurement and the natural Kr isotope ratios (⁸³Kr/⁸⁴Kr = 0.20175 and ⁸³Kr/⁸⁶Kr = 0.66474).^{42,43} In addition, we monitored ¹⁶⁷Er²⁺, ¹⁷¹Yb²⁺, and ¹⁷³Yb²⁺ at mass to charge ratios of 83.5, 85.5, and 86.5, which indicated there was negligible interference from doubly charged ions. The natural ratio of ⁸⁵Rb/⁸⁷Rb (2.5926) was used to correct for the isobaric interference of ⁸⁷Rb on ⁸⁷Sr utilizing the

exponential law and assuming that Rb undergoes the same mass bias as Sr.⁴⁴ Finally, the ⁸⁷Sr/⁸⁶Sr ratios were calculated and normalised to the interference-corrected ⁸⁶Sr/⁸⁸Sr ratio using the exponential law.

The isobaric interference of ¹⁴⁴Sm on ¹⁴⁴Nd must be corrected in order to obtain accurate ¹⁴⁷Sm/¹⁴⁴Nd and ¹⁴³Nd/¹⁴⁴Nd data by LA-MC-ICP-MS.^{15,27–30} Data reduction was performed offline using a Microsoft Excel macro. We used ¹⁴⁷Sm/¹⁴⁹Sm = 1.08680, ¹⁴⁴Sm/¹⁴⁹Sm = 0.22332, and ¹⁴⁶Nd/¹⁴⁴Nd = 0.7219.^{45–47} The

measured $^{147}\text{Sm}/^{149}\text{Sm}$ ratio was used to calculate the Sm fractionation factor (β_{Sm}) using the exponential law. The measured ^{147}Sm intensity was used to correct for the Sm interference on mass 144 using the natural $^{147}\text{Sm}/^{144}\text{Sm}$ ratio of 4.866559.⁴⁷ The interference-corrected $^{146}\text{Nd}/^{144}\text{Nd}$ ratio was then used to calculate the Nd fractionation factor (β_{Nd}). Finally, $^{143}\text{Nd}/^{144}\text{Nd}$ and $^{145}\text{Nd}/^{144}\text{Nd}$ ratios were normalised to $^{146}\text{Nd}/^{144}\text{Nd} = 0.7219$ using the exponential law; the $^{147}\text{Sm}/^{144}\text{Nd}$ ratio can also be calculated using the exponential law after correcting for the isobaric interference of ^{144}Sm on ^{144}Nd . The $^{147}\text{Sm}/^{144}\text{Nd}$ and $^{143}\text{Nd}/^{144}\text{Nd}$ ratios were then calibrated to the $^{147}\text{Sm}/^{144}\text{Nd}$ and $^{143}\text{Nd}/^{144}\text{Nd}$ ratios, respectively, obtained in one analysis of M659 vesuvianite during the same session.^{16,48,49}

2.3 Solution Sr and Sm–Nd isotope analysis

All chemistry procedures were performed in class 100 fume hoods located in a suite of class 1000 over-pressured clean rooms. Brief descriptions of the analytical techniques for the sample digestion, column chemistry, and mass spectrometry are given here and are provided elsewhere in detail.^{50–52} About 40–70 mg of powder of the vesuvianite samples and appropriate amounts of a ^{149}Sm – ^{150}Nd mixed spike solution were weighed (to 0.1 mg precision) into 7 mL Savillex PFA vials. The samples were dissolved in a mixture of 4 mL of 22 M HF, 2 mL of 14 M HNO_3 , and 0.2 mL of 70% m/m HClO_4 at 120 °C on a hotplate for one week. After cooling, the beakers were opened to dry at 100 °C and heated to 200 °C to evaporate HClO_4 . The residues were then dissolved in 2 mL of 14 M HNO_3 and dried, and this step was repeated once. Finally, the sample residues were treated with 6 M HCl, evaporated to dryness, and taken up in 1 mL of 2.5 M HCl before chemical separation. The first stage involved standard cation exchange chromatography for Rb and Sr purification. The REEs were eluted with 6 M HCl and further purified using Eichrom Ln resin (100–150 μm ; 2 mL) with 0.2 M HCl for Nd and 0.4 M HCl for Sm. The Sr and Sm–Nd fractions were collected in clean PFA beakers and evaporated to dryness, taken up with 0.1 mL of 2 M HCl, and diluted to 1.2 mL with 2% HNO_3 prior to MC-ICP-MS analysis.

All isotope measurements were carried out with a Neptune Plus MC-ICP-MS. A summary of the typical instrumental parameters and Faraday cup configurations for the Sr–Nd isotopic measurements is presented in Table 1. The Sr and Sm–Nd isotope data were acquired in static, multi-collector mode at low resolution. Aliquots of 150 ng g^{-1} NBS987 and 350 ng g^{-1} JNdi-1 Nd and Alfa Sm were used regularly to optimise the operational parameters and maximise the sensitivity of the instrument. The sample introduction system was rinsed with 2% HNO_3 to minimise memory effects between sample measurements. Procedural blanks were <100 pg Sr and 50 pg for Sm and Nd. $^{87}\text{Sr}/^{86}\text{Sr}$ and $^{143}\text{Nd}/^{144}\text{Nd}$ ratios were normalised to $^{86}\text{Sr}/^{88}\text{Sr} = 0.1194$ and $^{146}\text{Nd}/^{144}\text{Nd} = 0.7219$, respectively, using the exponential law. The Sm and Nd contents were calculated from the corrected $^{147}\text{Sm}/^{149}\text{Sm}$ and $^{150}\text{Nd}/^{144}\text{Nd}$ ratios, respectively, using the isotope dilution equation.

During the period of data acquisition, the analyses yielded $^{87}\text{Sr}/^{86}\text{Sr} = 0.710256 \pm 0.000014$ (2s; $n = 15$) for NBS987 and

$^{143}\text{Nd}/^{144}\text{Nd} = 0.512111 \pm 0.000009$ (2s; $n = 9$) for JNdi-1. Replicate analyses of the certified Chinese rock reference material GSR-3 basalt were conducted and yielded 0.704077 ± 0.000018 (2s; $n = 2$) for $^{87}\text{Sr}/^{86}\text{Sr}$, 0.512911 ± 0.000055 (2s; $n = 2$) for $^{143}\text{Nd}/^{144}\text{Nd}$, and 0.1205 for $^{147}\text{Sm}/^{144}\text{Nd}$, which are identical within uncertainty to the recommended values for this standard determined by TIMS or MC-ICP-MS.^{20,53}

In this study, the reported uncertainty (2s) represented external reproducibility (2SD) when the number of analysis times was more than 2, and 2s represented the within-run precision of each analysis (2SE) when the number of tests was only 1. The average of the within-run precision of two analysis (2SE) was used as the uncertainty for $n = 2$.

3. Sample descriptions

The vesuvianite samples investigated in this study are museum specimens (M6635, M784, M1377, M659, M660, M1439, M1450, and M6601; Institute of Geology and Geophysics, Chinese Academy of Sciences [IGGCAS], Beijing), were purchased from a mineral trader (Wilui, Hazlov, and Goodall specimens), or have been studied previously for trace elements (13MDL176).⁸ These 12 vesuvianite samples are from different countries (China, Myanmar, Russia, Czech Republic, and the USA). Brief details of the investigated vesuvianite samples are given in Table 2.

3.1 China

Vesuvianite samples M6635, M784, and M1377 were collected from the Saima alkaline complex located in northeastern China. The Saima alkaline complex consists of quartz-bearing syenites, alkaline volcanic rocks, and nepheline syenites. Field observations show that the nepheline syenites mainly intruded the Cambrian–Ordovician limestones and Precambrian marbles located within a narrow metamorphic belt.⁵⁴ Vesuvianite samples M6635 and M784 are about $8 \times 11 \times 4$ cm and $5 \times 8 \times 6$ cm large specimens, respectively. ID-TIMS analyses of six small crystal fragments of M6635 yielded a concordant $^{206}\text{Pb}/^{238}\text{U}$ age of 228.1 ± 0.5 Ma (2s), while the six aliquots of M784 yielded a concordant $^{206}\text{Pb}/^{238}\text{U}$ age of 224.8 ± 1.8 Ma (2s) in our previous study.¹² M1377 vesuvianite is an approximately $15 \times 10 \times 8$ cm large specimen, and LA-SF-ICP-MS data plotted on the Tera–Wasserburg diagram produced an intercept age of 225.0 ± 3.3 Ma (2s; $n = 20$).¹² Zhu *et al.*⁵⁴ measured the Sr–Nd isotopic compositions of Saima nepheline syenites using solution MC-ICP-MS and obtained initial $^{87}\text{Sr}/^{86}\text{Sr}$ ratios of 0.70804–0.70829 and negative $\varepsilon_{\text{Nd}}(t)$ values of -12.7 to -12.2 .

Vesuvianite samples M659, M660, and M1439 are about $5 \times 8 \times 3$ cm, $6 \times 10 \times 4$ cm, and $2 \times 1 \times 0.5$ cm large specimens, respectively. They were collected from a skarn exposed in the Dongpo ore field, Hunan Province, South China. The Dongpo ore field is in the western region of the Nanling Range and well-known for its large-scale W–Sn polymetallic deposits. The polymetallic mineralisation in the world-class Dongpo ore field is genetically related to the Qianlishan pluton.⁵⁵ The Qianlishan granitic complex intrudes into the Devonian sandstone and

Table 2 Details of the vesuvianite samples investigated in this study

Sample	Location	Host rock	Age (Ves; U–Pb)	$^{87}\text{Sr}/^{86}\text{Sr}$	$\epsilon_{\text{Nd}}(t)$	Provider	References
M6635 M784 M1377	Saima, Liaoning, China	Alkaline rock	228.1 ± 0.5 Ma 224.8 ± 1.8 Ma 225.0 ± 3.3 Ma	0.70804–0.70829 (whole rock)	–12.7 to –12.2 (whole rock)	IGGCAS museum	Wei <i>et al.</i> ; ¹² Zhu <i>et al.</i> ⁵⁴
M659 M660 M1439	Dongpo orefield, Hunan, China	Skarn	155.4 ± 2.0 Ma 156.5 ± 2.7 Ma 158.5 ± 3.1 Ma		–11.5 to –4.2 (whole rock; Qianlishan complex)	IGGCAS museum	Wei <i>et al.</i> ; ¹² Chen <i>et al.</i> ; ⁵⁶ Guo <i>et al.</i> ⁵⁷
M1450	Gupo Mountain, Guangxi, China	Skarn		0.7066 ± 0.0027 (whole rock; granite)		IGGCAS museum	Gu <i>et al.</i> ⁵⁸
M6601	Lanigou, Guangxi, China		93.3 ± 2.5 Ma			IGGCAS museum	Wei <i>et al.</i> ¹²
13MDL176	Mogok metamorphic belt, Myanmar	Calc-silicate rock	33.7 ± 2.9 Ma ^a			Guo Shun	Guo <i>et al.</i> ⁸
Wilui	Vilyui (Wiluy) River, Yakutia, Russia	Skarn	255.5 ± 0.6 Ma	0.7090–0.7095 (whole rock; limestone)		E-Bay	Wei <i>et al.</i> ; ¹² Alexeev <i>et al.</i> ⁶³
Hazlov	Cheb District, Karlovy Vary Region, Czech Republic	Skarn	325 ± 22 Ma ^a	0.7051–0.7129 (whole rock; granitoids)		E-Bay	Janoušek <i>et al.</i> ⁶⁴
Goodall	Sanford deposit, Maine, USA	Skarn				E-Bay	

^a Our unpublished data.

limestone.⁵⁶ Our previous study reported that M659, M660, and M1439 yield intercept U–Pb ages of 155.4 ± 2.0 Ma (2s; $n = 21$), 156.5 ± 2.7 Ma (2s; $n = 21$), and 158.5 ± 3.1 Ma (2s; $n = 19$), respectively, in the Tera–Wasserburg diagram.¹² The whole-rock $\epsilon_{\text{Nd}}(t)$ values of the Qianlishan granitic complex gave a wide range from –11.5 to –4.2.^{56,57}

Vesuvianite sample M1450 is an about 5 × 4 × 5 cm large specimen. It was collected from the skarn W–Sn ore deposits in the Guposhan ore field, Guangxi Province, which is located in the southwestern Nanling region. Gu *et al.*⁵⁸ divided the Guposhan pluton into three units, namely the East unit (160.8 ± 1.6 Ma), the West unit (165.0 ± 1.9 Ma), and the Lisong unit (163.0 ± 1.3 Ma). The $^{87}\text{Sr}/^{86}\text{Sr}$ ratios of scheelite hosted in skarn type-ores vary from 0.70277 to 0.71471, which retained the Sr isotopic signature of the related granites (0.7066 ± 0.0027).^{58,59}

Vesuvianite sample M6601 is an about 4 × 5 × 4 cm large specimen. However, it is not known from which deposit in Guangxi Province vesuvianite sample M6601 was collected.

3.2 Myanmar

Vesuvianite sample 13MDL176 is hosted in a calc-silicate rock from the Mogok metamorphic belt (MMB), Myanmar, which was supplied by Prof Shun Guo.⁸ Two Cainozoic metamorphic

events affected the MMB. One ended at *ca.* 59 Ma, and another possibly lasted from 47 to 29 Ma.⁶⁰ Our unpublished LA-SF-ICP-MS U–Pb data show that nineteen analyses yield an intercept age of 33.7 ± 2.9 Ma (2s) in the Tera–Wasserburg diagram. Formation of the MMB calc-silicate minerals has been attributed to an external fluid phase that reacted with early-stage calcite.⁸ The ore-forming magma and fluid are thought to be contributed to Palaeocene–Eocene crustal melting of a meta-sedimentary protolith;⁶¹ however, no Nd isotope data are available for whole-rock or accessory mineral samples.

3.3 Russia

Wilui vesuvianite is an approximately 1 × 1.5 × 2 cm dark green specimen with well-developed prism faces and double termination. It was collected from rodingitized Mg–Ca–skarn at the contact between the Siberian Traps and Ordovician carbonate rocks. The genesis of the Wiluy (Wilui) deposit was traditionally connected with metamorphism of sedimentary rocks induced by the intrusion of basic dikes and sills of the Siberian Traps series.⁶² Alexeev *et al.*⁶³ presented the $^{87}\text{Sr}/^{86}\text{Sr}$ values of 0.7090–0.7095 for the Palaeozoic limestones of the Siberian Platform.

3.4 Czech Republic

Vesuvianite sample Hazlov is an about $6 \times 6 \times 4$ cm large specimen. It was collected from skarn at the Bohemian Massif in Cheb District, Karlovy Vary region, Czech Republic. The sample yield intercept U–Pb ages of 325 ± 22 Ma ($2s$; $n = 21$) in the Tera–Wasserburg diagram from our unpublished data. Janoušek *et al.*⁶⁴ reported Sr isotope data for granitoids aged *ca.* 330 Ma from the Central Bohemian Pluton, which experienced medium- to high-grade metamorphism during the Variscan Orogeny (380–310 Ma). The granitoids have a wide range of Sr isotopic compositions (0.7051–0.7129).

3.5 USA

Vesuvianite sample Goodall is an approximately $6 \times 5 \times 3$ cm dark green specimen and from skarn in the Sanford deposit, Maine, USA.⁶⁵ No detailed Sr–Nd isotopic data have been reported for this deposit so far.

4. Sr–Nd isotope analysis of the in-house standard

Currently, there is no vesuvianite isotopic standard for *in situ* Sr–Nd isotope analysis. To check the reliability of our methods, two in-house vesuvianite standards (M6635 & M659) were analysed by solution and laser ablation methods. Trace element contents of samples M6635 and M659 are summarised in Table S1.†

M6635 vesuvianite has high Sr ($2823 \pm 306 \mu\text{g g}^{-1}$) and low Rb ($0.35 \pm 0.10 \mu\text{g g}^{-1}$) contents (Table S1.†). Three LA-MC-ICP-MS analytical sessions of M6635 vesuvianite yielded relatively homogeneous $^{87}\text{Sr}/^{86}\text{Sr}$ ratios of 0.70825 ± 0.00005 ($2s$; $n = 15$) to 0.70829 ± 0.00008 ($2s$; $n = 14$), with an average of 0.70826 ± 0.00007 ($2s$; $n = 44$) (Fig. 1a), which is consistent with the solution MC-ICP-MS average of 0.708265 ± 0.000030 ($2s$; $n = 3$). The Sr isotopic composition of M6635 vesuvianite is

homogeneous; therefore, it was used to externally calibrate the other vesuvianite samples during this study.

Trace element mass fractions of M659 vesuvianite determined by LA-ICP-MS show large variations and high Nd ($413 \pm 560 \mu\text{g g}^{-1}$) with moderate Sm ($53 \pm 83 \mu\text{g g}^{-1}$) mass fractions (Table S1.†). The $^{143}\text{Nd}/^{144}\text{Nd}$ ratios of M659 vesuvianite varied from 0.512063 ± 0.000036 ($2s$; $n = 15$) to 0.512091 ± 0.000055 ($2s$; $n = 15$) over the course of three LA analytical sessions, and the $^{147}\text{Sm}/^{144}\text{Nd}$ ratios varied from 0.0774 ± 0.0195 ($2s$; $n = 15$) to 0.0804 ± 0.0112 ($2s$; $n = 15$), with averages of 0.0787 ± 0.0152 ($2s$; $n = 45$) and 0.512076 ± 0.000051 ($2s$; $n = 45$) (Fig. 1b). The calculated initial $^{143}\text{Nd}/^{144}\text{Nd}$ ratios of 45 analyses only show limited variation (0.511996 ± 0.000048 ; $2s$). The average $^{145}\text{Nd}/^{144}\text{Nd}$ ratio of 0.348400 ± 0.000038 ($2s$; $n = 45$) is consistent with the recommended value.⁶⁶ Two aliquots of M659 vesuvianite grains were selected for solution analyses, yielding an average $^{143}\text{Nd}/^{144}\text{Nd}$ ratio of 0.512118 ± 0.000012 ($2s$; $n = 2$) and an average $^{147}\text{Sm}/^{144}\text{Nd}$ ratio of 0.0792, which are consistent with the LA-MC-ICP-MS values. The corresponding $\epsilon_{\text{Nd}}(t)$ value for M659 vesuvianite is -7.8 ± 0.2 ($2s$) for the solution analyses, which agrees well with the LA value of -8.6 ± 0.9 ($2s$) based on the U–Pb age of 155.4 ± 2.0 Ma ($2s$).¹²

In summary, laser ablation of M6635 gives identical Sr isotopic ratios, and M659 exhibits minor variations of $^{147}\text{Sm}/^{144}\text{Nd}$ values with relatively homogeneous Nd isotopic ratios. The results of these two in-house vesuvianite standards are consistent with the solution technique values within analytical errors, indicating that our analytical protocol is reliable. Thus, M6635 and M659 vesuvianite were used for external correction during *in situ* laser ablation analysis for Sr and Nd isotopic compositions, respectively.

5. Applications

Trace element contents and Sr–Nd isotopic data (obtained by LA-MC-ICP-MS) are summarised in Tables S1.† and 3,

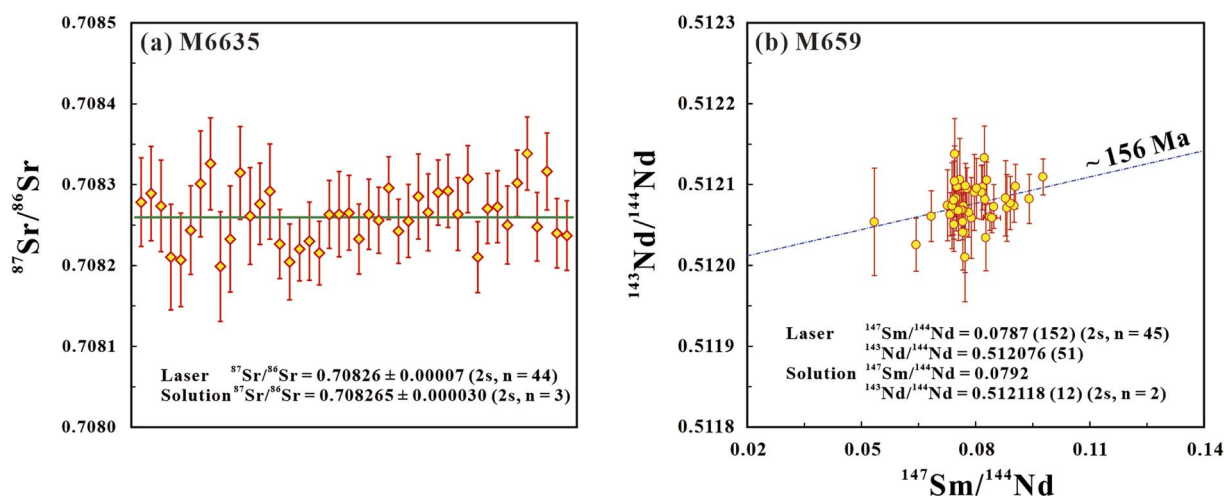


Fig. 1 (a) *In situ* Sr isotopic analyses of in-house vesuvianite standard of M6635. (b) *In situ* Sm–Nd isotopic analyses of in-house vesuvianite standard of M659. Error bars are 2 sigma.

Table 3 Strontium and Sm–Nd isotope data for vesuvianite obtained by LA-MC-ICP-MS

Sample	<i>n</i>	⁸⁷ Sr/ ⁸⁶ Sr (±2s)	<i>n</i>	¹⁴⁷ Sm/ ¹⁴⁴ Nd (±2s)	2RSD (%)	¹⁴³ Nd/ ¹⁴⁴ Nd (±2s)	¹⁴³ Nd/ ¹⁴⁴ Nd(<i>t</i>) (±2s)	ε _{Nd} (<i>t</i>) ^a (±2s)	¹⁴⁵ Nd/ ¹⁴⁴ Nd (±2s)
M6635 (~228 Ma)									
1	14	0.70829 (8)	15	0.0352 (102)	28.94	0.511796 (37)	0.511743 (31)	–11.7 (0.6)	0.348403 (12)
2	15	0.70825 (5)	15	0.0427 (47)	11.10	0.511798 (29)	0.511734 (29)	–11.9 (0.6)	0.348403 (16)
3	15	0.70827 (7)	15	0.0349 (82)	23.42	0.511786 (27)	0.511734 (26)	–11.9 (0.5)	0.348408 (17)
Average	44	0.70826 (7)	45	0.0376 (107)	28.39	0.511793 (32)	0.511737 (29)	–11.9 (0.6)	0.348405 (15)
M784 (~224 Ma)									
1	15	0.70827 (6)	15	0.0428 (255)	59.71	0.511806 (47)	0.511743 (25)	–11.8 (0.5)	0.348393 (23)
2	15	0.70826 (5)	15	0.0556 (73)	13.15	0.511807 (44)	0.511725 (46)	–12.2 (0.9)	0.348385 (26)
3	15	0.70826 (7)	15	0.0348 (86)	24.63	0.511788 (39)	0.511737 (36)	–12.0 (0.7)	0.348407 (19)
Average	45	0.70826 (6)	45	0.0444 (234)	52.79	0.511800 (46)	0.511735 (39)	–12.0 (0.8)	0.348395 (29)
M1377 (~225 Ma)									
1	15	0.70821 (7)	15	0.0531 (102)	19.17	0.511823 (74)	0.511745 (68)	–11.8 (1.3)	0.348396 (22)
2	15	0.70824 (6)	15	0.0561 (103)	18.44	0.511816 (73)	0.511733 (71)	–12.0 (1.4)	0.348386 (26)
3	15	0.70823 (4)	15	0.0560 (111)	19.80	0.511816 (58)	0.511734 (51)	–12.0 (1.0)	0.348398 (42)
Average	45	0.70823 (6)	45	0.0550 (107)	19.41	0.511819 (68)	0.511737 (64)	–11.9 (1.2)	0.348393 (32)
M659 (~156 Ma)									
1			15	0.0804 (112)	13.96	0.512073 (45)	0.511991 (43)	–8.7 (0.8)	0.348398 (23)
2			15	0.0774 (195)	25.16	0.512063 (36)	0.511984 (34)	–8.8 (0.7)	0.348390 (36)
3			15	0.0785 (142)	18.14	0.512091 (55)	0.512012 (52)	–8.3 (1.0)	0.348412 (41)
Average			45	0.0787 (152)	19.33	0.512076 (51)	0.511996 (48)	–8.6 (0.9)	0.348400 (38)
M660 (~156 Ma)									
1			15	0.0696 (324)	46.49	0.512098 (93)	0.512027 (80)	–8.0 (1.6)	0.348397 (52)
2			15	0.0897 (435)	48.51	0.512110 (69)	0.512018 (54)	–8.2 (1.1)	0.348401 (38)
3			15	0.0770 (173)	22.43	0.512114 (59)	0.512035 (61)	–7.9 (1.2)	0.348404 (43)
Average			45	0.0788 (362)	45.99	0.512107 (74)	0.512027 (66)	–8.0 (1.3)	0.348401 (44)
M1439 (~158 Ma)									
1			14	0.1287 (121)	9.41	0.512308 (123)	0.512174 (126)	–5.1 (2.5)	0.348364 (65)
2			15	0.1227 (367)	29.91	0.512252 (109)	0.512125 (98)	–6.0 (1.9)	0.348378 (61)
3			15	0.1366 (181)	13.28	0.512235 (72)	0.512093 (69)	–6.7 (1.3)	0.348398 (65)
Average			44	0.1294 (269)	20.81	0.512264 (118)	0.512130 (118)	–5.9 (2.3)	0.348380 (68)
13MDL176 (~34 Ma)									
1			15	0.0848 (223)	26.27	0.511775 (76)	0.511756 (74)	–16.4 (1.4)	0.348395 (44)
2			15	0.0916 (515)	56.29	0.511735 (99)	0.511715 (90)	–17.2 (1.7)	0.348380 (33)
3			15	0.0855 (274)	32.05	0.511758 (54)	0.511739 (53)	–16.7 (1.0)	0.348401 (46)
Average			45	0.0873 (358)	40.98	0.511756 (83)	0.511737 (80)	–16.7 (1.6)	0.348392 (44)
M1450									
1	14	0.70816 (14)							
2	15	0.70815 (5)							
3	15	0.70817 (9)							
Average	44	0.70816 (10)							
M6601									
1	13	0.70993 (72)							
2	10	0.70929 (51)							
3	11	0.70958 (54)							
Average	34	0.70962 (79)							
Wilui									
1	15	0.70905 (60)							
2	20	0.70875 (21)							
Average	35	0.70888 (52)							
Hazlov									
1	15	0.70925 (39)							
2	16	0.70909 (49)							
3	15	0.70901 (36)							
Average	46	0.70912 (46)							

Table 3 (Contd.)

Sample	<i>n</i>	⁸⁷ Sr/ ⁸⁶ Sr (±2s)	<i>n</i>	¹⁴⁷ Sm/ ¹⁴⁴ Nd (±2s)	2RSD (%)	¹⁴³ Nd/ ¹⁴⁴ Nd (±2s)	¹⁴³ Nd/ ¹⁴⁴ Nd(<i>t</i>) (±2s)	$\epsilon_{\text{Nd}}(t)^a$ (±2s)	¹⁴⁵ Nd/ ¹⁴⁴ Nd (±2s)
Goodall									
1	15	0.71018 (40)							
2	16	0.70945 (32)							
Average	31	0.70980 (82)							

$$^a \epsilon_{\text{Nd}}(t) = \left[\frac{(\text{}^{143}\text{Nd}/\text{}^{144}\text{Nd})_{\text{sample}} - (\text{}^{147}\text{Sm}/\text{}^{144}\text{Nd})_{\text{sample}} \times (e^{\lambda t} - 1)}{(\text{}^{143}\text{Nd}/\text{}^{144}\text{Nd})_{\text{CHUR}} - (\text{}^{147}\text{Sm}/\text{}^{144}\text{Nd})_{\text{CHUR}} \times (e^{\lambda t} - 1)} - 1 \right] \times 10^4; \lambda^{147}\text{Sm} = 6.54 \times 10^{-10} \text{ y}^{-1} \text{ (Lugmair and Marti}^{69}); (\text{}^{147}\text{Sm}/\text{}^{144}\text{Nd})_{\text{CHUR}} = 0.1967 \text{ (Jacobsen and Wasserburg}^{70}); (\text{}^{143}\text{Nd}/\text{}^{144}\text{Nd})_{\text{CHUR}} = 0.512638 \text{ (Goldstein et al.}^{71}).$$

respectively. The Sr–Nd isotopic data for vesuvianite crystal chips obtained by solution MC-ICP-MS are listed in Table 4. More detailed information regarding the Sr and Sm–Nd isotope data can be found in the online ESI (Tables S2 and S3†).

5.1 China

5.1.1 Saima alkaline complex, liaoning province. M6635 vesuvianite has high Nd ($1547 \pm 245 \mu\text{g g}^{-1}$) and moderate Sm ($88 \pm 15 \mu\text{g g}^{-1}$) contents (Table S1†). The chondrite-normalised REE pattern (Fig. 2a) exhibits strong LREE enrichment and large LREE/heavy REE (HREE) fractionation ($[\text{La}/\text{Lu}]_{\text{N}} = 5414 \pm 1466$). ¹⁴³Nd/¹⁴⁴Nd ratios of M6635 vesuvianite vary from 0.511786 ± 0.000027 (2s; *n* = 15) to 0.511798 ± 0.000029 (2s; *n* = 15), with an average of 0.511793 ± 0.000032 (2s; *n* = 45), and ¹⁴⁷Sm/¹⁴⁴Nd ratios ranged from 0.0349 ± 0.0082 (2s; *n* = 15) to 0.0427 ± 0.0047 (2s; *n* = 15), with an average of 0.0376 ± 0.0107 (2s; *n* = 45) (Table 3 and Fig. 4a). The calculated initial ¹⁴³Nd/¹⁴⁴Nd ratios of forty-five analyses show only limited variation with a mean value of 0.511737 ± 0.000029 (2s). The average ¹⁴⁵Nd/¹⁴⁴Nd ratio of 0.348405 ± 0.000015 (2s; *n* = 45; Table 3) is in close agreement with the recommended value of 0.348415.⁶⁶ Two separate aliquots of M6635 vesuvianite analysed by solution MC-ICP-MS yielded ¹⁴⁷Sm/¹⁴⁴Nd and ¹⁴³Nd/¹⁴⁴Nd values of 0.0427 and 0.511798 ± 0.000010 (2s), respectively (Table 4). These solution-based data are within analytical uncertainty of the LA-MC-ICP-MS values. The corresponding $\epsilon_{\text{Nd}}(t)$ value for M6635 vesuvianite is -11.9 ± 0.2 (2s) for the solution analyses, which is consistent with the LA-MC-ICP-MS value of -11.9 ± 0.6 (2s) based on the M6635 vesuvianite U–Pb age (228.1 ± 0.5 Ma; 2s)¹² (Table 4).

The M784 vesuvianite has high Sr ($4632 \pm 128 \mu\text{g g}^{-1}$), low Rb ($0.47 \pm 0.10 \mu\text{g g}^{-1}$), and moderate Nd ($469 \pm 195 \mu\text{g g}^{-1}$) and Sm ($44 \pm 15 \mu\text{g g}^{-1}$) contents (Table S1†). The chondrite-normalised REE pattern (Fig. 2a) exhibits strong LREE enrichment and LREE/HREE fractionation ($[\text{La}/\text{Lu}]_{\text{N}} = 1372 \pm 904$). The ⁸⁷Sr/⁸⁶Sr ratios obtained by LA-MC-ICP-MS during three sessions were homogeneous and varied from 0.70826 ± 0.00007 (2s; *n* = 15) to 0.70827 ± 0.00006 (2s; *n* = 15), with an average of 0.70826 ± 0.00006 (2s; *n* = 45) (Table 3 and Fig. 3a). This result is consistent with the solution MC-ICP-MS average value of 0.708250 ± 0.000016 (2s; *n* = 3; Table 4). The M784 vesuvianite analysed by LA-MC-ICP-MS yielded ¹⁴⁷Sm/¹⁴⁴Nd and ¹⁴³Nd/¹⁴⁴Nd ratios of 0.0348–0.0556 and 0.511788–0.511807,

respectively, with averages of 0.0444 ± 0.0234 and 0.511800 ± 0.000046 (2s; *n* = 45; Table 3 and Fig. 4a). The calculated initial ¹⁴³Nd/¹⁴⁴Nd ratio shows limited variation (0.511735 ± 0.000039 ; 2s; *n* = 45). The ¹⁴⁵Nd/¹⁴⁴Nd ratios has an average value of 0.348395 ± 0.000029 (2s; *n* = 45; Table 3), which is consistent with the recommended value.⁶⁶ Two fragments of M784 were analysed by solution MC-ICP-MS and yielded an average ¹⁴³Nd/¹⁴⁴Nd ratio of 0.511792 ± 0.000008 (2s; *n* = 2) and ¹⁴⁷Sm/¹⁴⁴Nd ratio of 0.0389 (Table 4). These data are in good agreement with the LA-MC-ICP-MS results. The corresponding $\epsilon_{\text{Nd}}(t)$ value for M784 vesuvianite is -12.0 ± 0.1 (2s), which is identical to the LA-MC-ICP-MS value of -12.0 ± 0.8 (2s), using the U–Pb age of 224.8 ± 1.8 Ma (2s) for M784 vesuvianite¹² (Table 4).

Like the M6635 and M784 vesuvianites, LA-ICP-MS analyses indicate that the M1377 vesuvianite is also homogeneous with respect to trace element abundances and has particularly high Sr ($3420 \pm 224 \mu\text{g g}^{-1}$), low Rb ($0.14 \pm 0.03 \mu\text{g g}^{-1}$), high Nd ($571 \pm 46 \mu\text{g g}^{-1}$), and moderate Sm ($50 \pm 5 \mu\text{g g}^{-1}$) contents (Table S1†). The chondrite-normalised REE pattern (Fig. 2a) shows that this sample is LREE enriched and exhibits strong LREE/HREE fractionation ($[\text{La}/\text{Lu}]_{\text{N}} = 2220 \pm 824$). The LA-MC-ICP-MS ⁸⁷Sr/⁸⁶Sr data are homogeneous and range from 0.70821 ± 0.00007 (2s; *n* = 15) to 0.70824 ± 0.00006 (2s; *n* = 15), with an average of 0.70823 ± 0.00006 (2s; *n* = 45) (Table 3 and Fig. 3a), which is consistent with the value of 0.708243 ± 0.000011 (2s; *n* = 2) obtained by solution MC-ICP-MS (Table 4). M1377 vesuvianite exhibits slight variations in ¹⁴⁷Sm/¹⁴⁴Nd and limited variations in ¹⁴³Nd/¹⁴⁴Nd ratios of 0.0531–0.0561 and 0.511816–0.511823, respectively, with averages of 0.0550 ± 0.0107 and 0.511819 ± 0.000068 (2s; *n* = 45; Table 3 and Fig. 4a). The average ¹⁴⁵Nd/¹⁴⁴Nd ratio of 0.348393 ± 0.000032 (2s; *n* = 45) obtained in three sessions is identical to the recommended value of 0.348415 (Table 3).⁶⁶ The solution-based ¹⁴⁷Sm/¹⁴⁴Nd ratio of 0.0322 and ¹⁴³Nd/¹⁴⁴Nd ratio of 0.511781 ± 0.000008 (2s; *n* = 1) are somewhat lower than, but still consistent with (*i.e.*, within uncertainty), the LA results (Table 4). Based on the M1377 vesuvianite U–Pb age of 225.0 ± 3.3 Ma (2s),¹² the corresponding $\epsilon_{\text{Nd}}(t)$ value for M1377 vesuvianite is -12.0 ± 0.1 (2s), which is within uncertainty of the LA-MC-ICP-MS value of -11.9 ± 1.2 (2s) (Table 4).

The LA- and solution-based MC-ICP-MS Sr–Nd isotopic data for these three vesuvianite samples agree well with previously

Table 4 Strontium and Sm–Nd isotope data for vesuvianite obtained by solution MC-ICP-MS

Sample	$^{87}\text{Sr}/^{86}\text{Sr}$	$2s^a$	Sm ($\mu\text{g g}^{-1}$)	Nd ($\mu\text{g g}^{-1}$)	$^{147}\text{Sm}/^{144}\text{Nd}$	$^{143}\text{Nd}/^{144}\text{Nd}$	$2s^a$	$\epsilon_{\text{Nd}}(t)$ ($\pm 2s$)
M6635 (~228 Ma)								
1	0.708277	0.000010	65.7	1022	0.0389	0.511795	0.000009	−11.9 (0.2)
2	0.708248	0.000016	64.7	841	0.0465	0.511801	0.000011	−12.0 (0.2)
3	0.708269	0.000013						
Average	0.708265		65.2	931	0.0427	0.511798		−11.9
2s	0.000030					0.000010		0.2
M784 (~224 Ma)								
1	0.708259	0.000016	73.5	1136	0.0391	0.511801	0.000009	−11.8 (0.2)
2	0.708248	0.000015	73.5	1150	0.0386	0.511783	0.000006	−12.1 (0.1)
3	0.708243	0.000013						
Average	0.708250		73.5	1143	0.0389	0.511792		−12.0
2s	0.000016					0.000008		0.1
M1377 (~225 Ma)								
1	0.708246	0.000011	94.0	1764	0.0322	0.511781	0.000008	−12.0 (0.1)
2	0.708240	0.000012						
Average	0.708243							
2s	0.000011							
M659 (~156 Ma)								
1			84.6	648	0.0788	0.512126	0.000013	−7.7 (0.3)
2			71.3	542	0.0795	0.512111	0.000010	−8.0 (0.2)
Average			77.9	595	0.0792	0.512118		−7.8
2s						0.000012		0.2
M660 (~156 Ma)								
1			71.7	495	0.0876	0.512132	0.000013	−7.7 (0.2)
2			32.6	206	0.0955	0.512133	0.000016	−7.8 (0.3)
Average			52.2	351	0.0915	0.512133		−7.8
2s						0.000014		0.3
M1439 (~158 Ma)								
1			30.1	145	0.1255	0.512287	0.000023	−5.4 (0.4)
13MDL176 (~34 Ma)								
1			31.9	206	0.0938	0.511777	0.000014	−16.4 (0.3)
M1450								
1	0.708162	0.000014						
M6601								
1	0.709796	0.000014						
Wilui								
1	0.708716	0.000013						
2	0.708717	0.000016						
3	0.708736	0.000009						
4	0.708726	0.000015						
Average	0.708724							
2s	0.000019							
Hazlov								
1	0.709177	0.000014						
Goodall								
1	0.710196	0.000018						

^a 2s: 2 standard in-run errors.

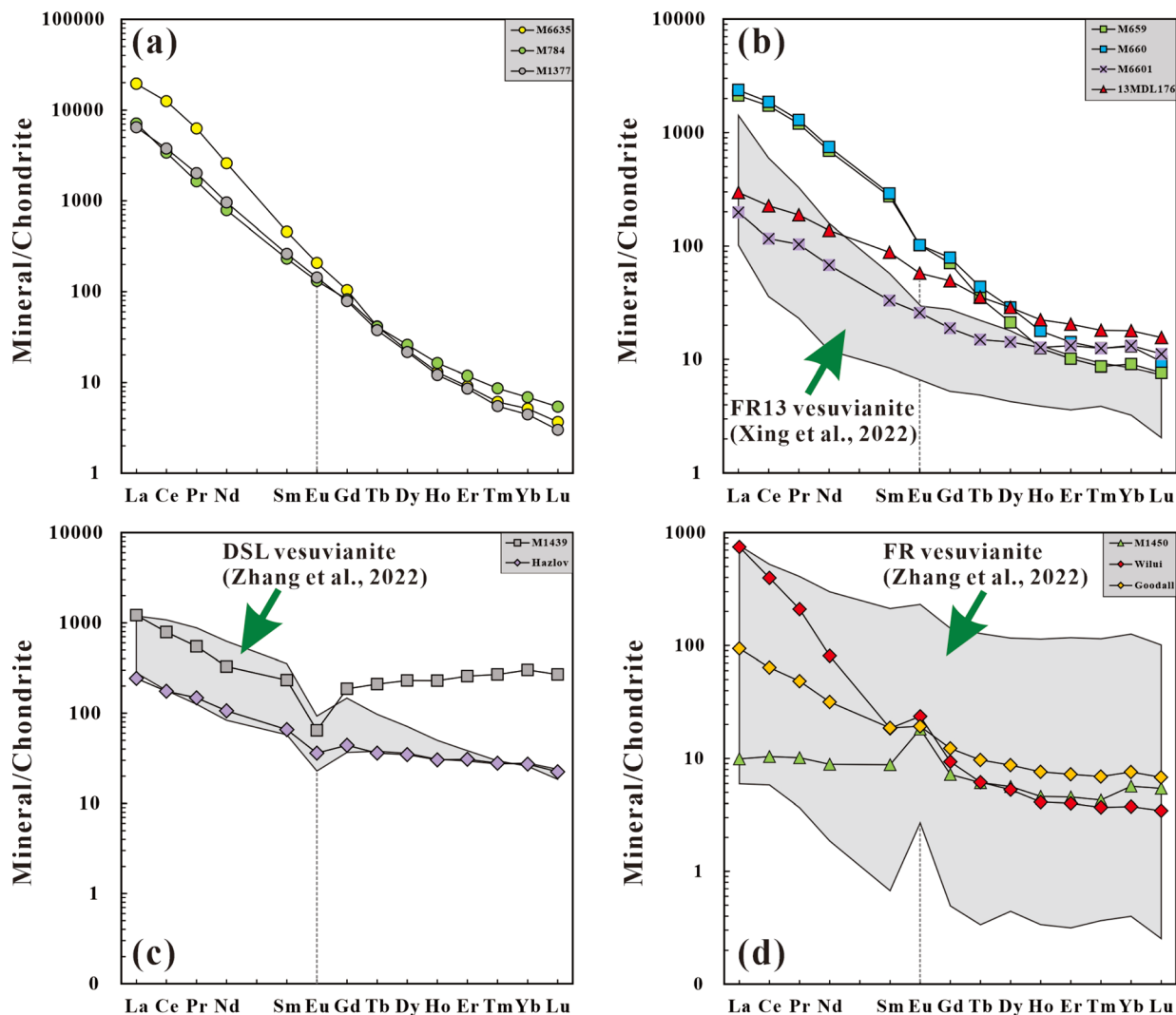


Fig. 2 Chondrite-normalised REE patterns for the 12 vesuvianite samples. Normalisation values are from McDonough and Sun.⁶⁷ Four subgroups can be identified: (a) high REE contents with high $(La/Lu)_N$ values; (b) no obvious Eu anomalies; (c) negative Eu anomalies; and (d) positive Eu anomalies. The fields for the FR13, DSL, and FR vesuvianite samples are from Xing *et al.*¹³ and Zhang *et al.*¹⁴

reported Sr–Nd isotope data of the nepheline syenites, which have initial $^{87}\text{Sr}/^{86}\text{Sr}$ ratios of 0.70804–0.70829 and negative $\varepsilon_{\text{Nd}}(t)$ values of -12.7 to -12.2 .⁵⁴ Therefore, *in situ* analyses of Sr–Nd isotopes of vesuvianite, coupled with those of other accessory minerals (*e.g.*, apatite and titanite), field observations, and whole-rock geochemical data can provide insights into the origins and petrogenesis of alkaline igneous rocks.

5.1.2 Dongpo ore field, Hunan Province. Trace element contents of vesuvianite samples M660 and M1439 determined by LA-ICP-MS exhibit large variations. M660 has high Nd and moderate Sm contents, with Nd = 76–921 $\mu\text{g g}^{-1}$ and Sm = 6–131 $\mu\text{g g}^{-1}$ (Table S1†). It also has variable Eu anomalies ($\text{Eu}/\text{Eu}^* = 0.4\text{--}3.5$). Similar to vesuvianite sample FR13 from the skarn Sn deposit in southern Hunan Province,¹³ the chondrite-normalised REE pattern of M660 vesuvianite is also highly fractionated and LREE enriched (Fig. 2b). M1439 vesuvianite also has heterogeneous Nd ($196 \pm 298 \mu\text{g g}^{-1}$) and Sm ($45 \pm 77 \mu\text{g g}^{-1}$) contents (Table S1†). The chondrite-normalised REE

pattern (Fig. 2c) exhibits slight LREE enrichment. M1439 vesuvianite also has a negative Eu anomaly, which is similar to that of DSL vesuvianite from the Dashunlong Sn deposit in the Nanling Range, southern China.¹⁴ These three samples (including M659) have low Sr content ($\sim 20 \mu\text{g g}^{-1}$; Table S1†), which are not suitable for *in situ* Sr isotope analysis.

The LA-MC-ICP-MS Sm–Nd isotope data for M660 vesuvianite revealed variations in $^{147}\text{Sm}/^{144}\text{Nd}$ and $^{143}\text{Nd}/^{144}\text{Nd}$ from 0.0696 to 0.0897 (average = 0.0788 ± 0.0362 ; 2s; $n = 45$) and 0.512098 to 0.512114 (average = 0.512107 ± 0.000074 ; 2s; $n = 45$), respectively (Table 3 and Fig. 4b). The average $^{145}\text{Nd}/^{144}\text{Nd}$ ratio obtained in three sessions was 0.348401 ± 0.000044 (2s; $n = 45$), which is consistent with the recommended value (Table 3).⁶⁶ The solution-based $^{147}\text{Sm}/^{144}\text{Nd}$ and $^{143}\text{Nd}/^{144}\text{Nd}$ ratios are 0.0915 and 0.512133 ± 0.000014 (2s; $n = 2$), respectively (Table 4). The LA- and solution-based Sm–Nd isotopic data are in good agreement. The calculated $\varepsilon_{\text{Nd}}(t)$ value based on the U–Pb age of

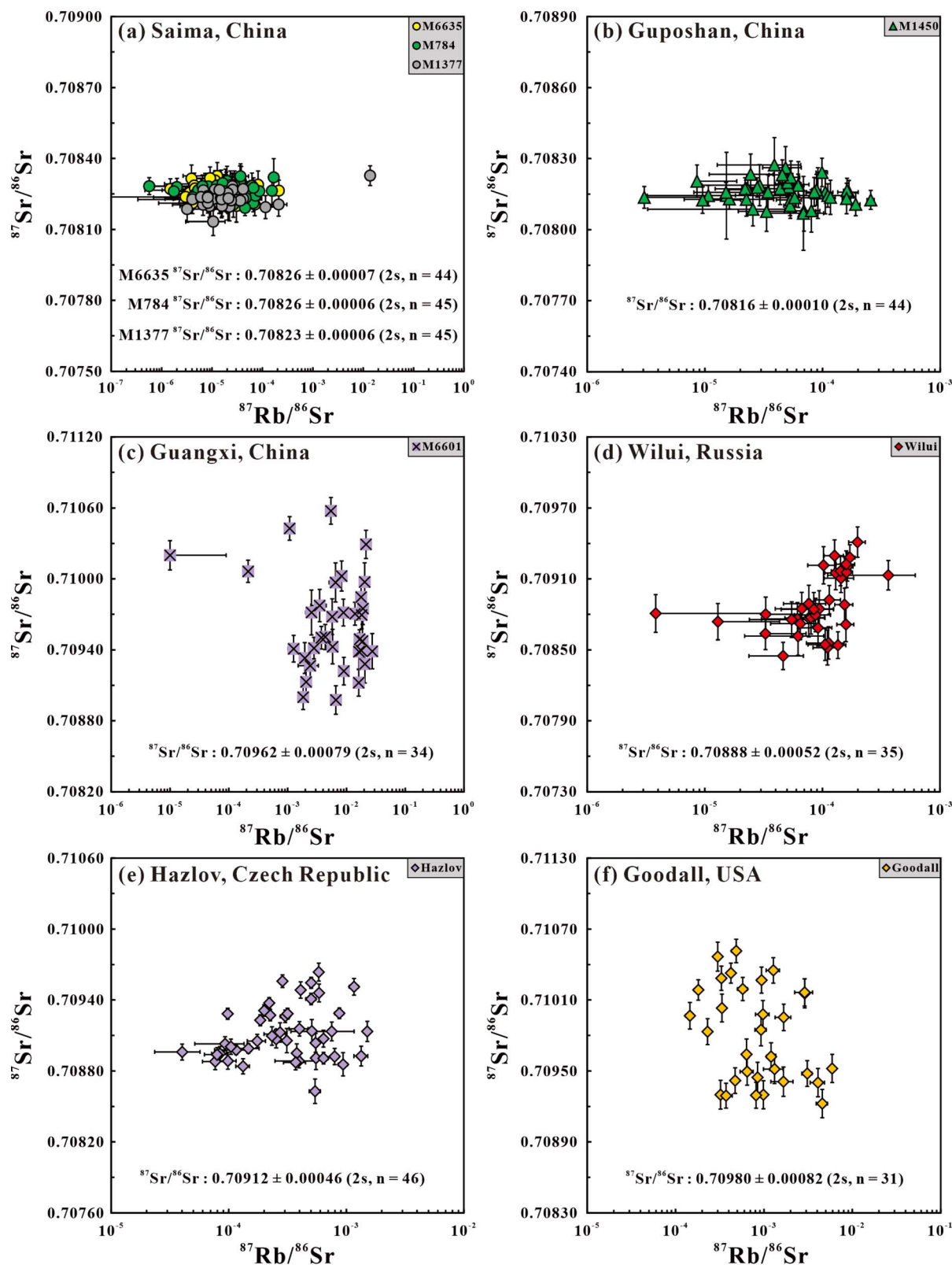


Fig. 3 Measured $^{87}\text{Rb}/^{86}\text{Sr}$ – $^{87}\text{Sr}/^{86}\text{Sr}$ ratios of eight vesuvianite samples obtained during multiple analytical sessions. (a) M6635, M784, and M1377 from Saima, China; (b) M1450 from Guposhan, China; (c) M6601 from Guangxi, China; (d) Wilui from Russia; (e) Hazlov from Czech Republic; and (f) Goodall from USA. Error bars are 2 sigma.

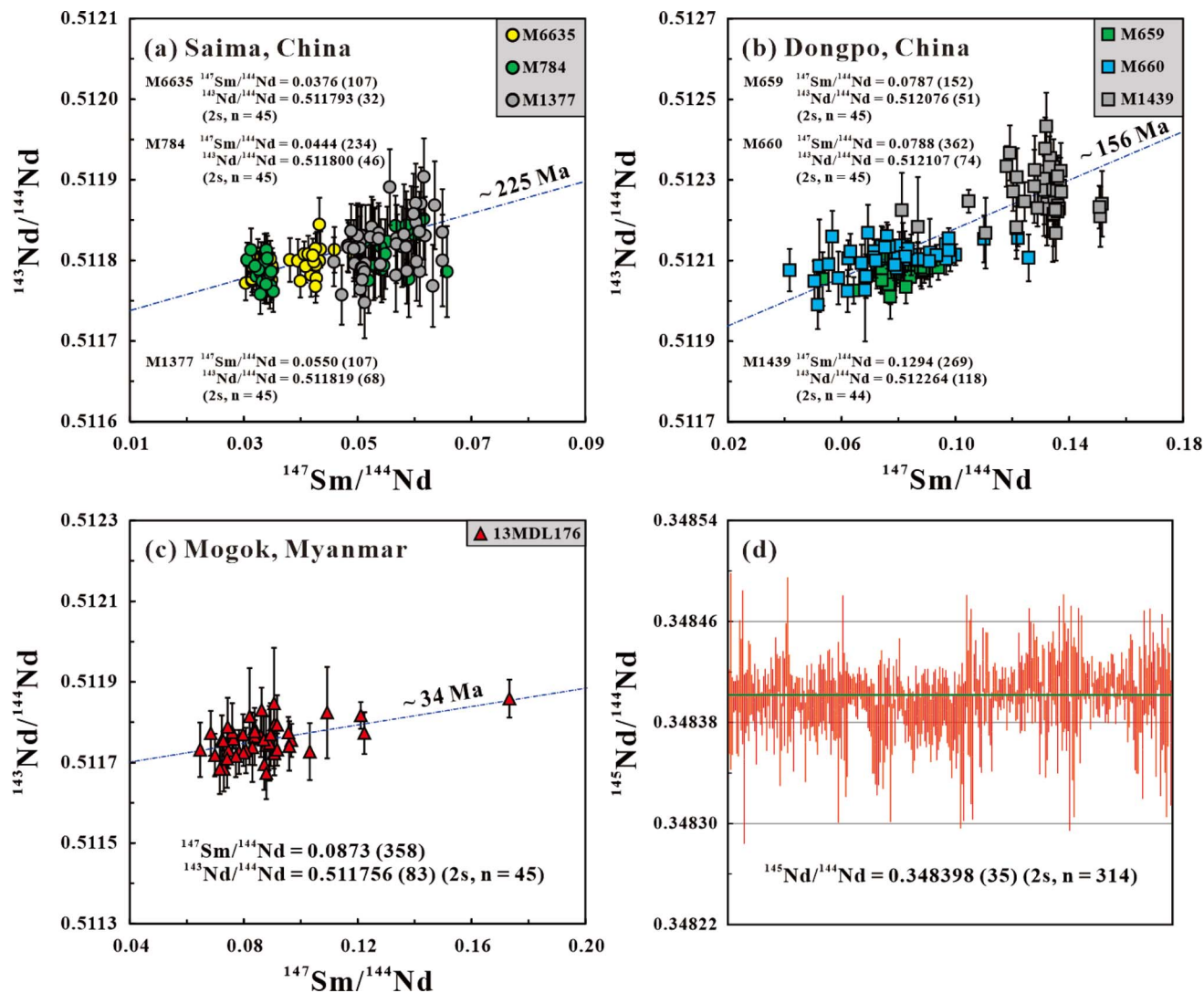


Fig. 4 Plots of $^{147}\text{Sm}/^{144}\text{Nd}$ – $^{143}\text{Nd}/^{144}\text{Nd}$ ratios for the studied vesuvianite samples. (a) M6635, M784, and M1377 from Saima, China; (b) M659, M660, and M1439 from Dongpo, China; and (c) 13MDL176 from Mogok, Myanmar. (d) $^{145}\text{Nd}/^{144}\text{Nd}$ ratios of all data obtained during laser ablation analysis. n = number of analyses. All error bars are 2 sigma.

156.5 ± 2.7 Ma (2s)¹² is -7.8 ± 0.3 (2s), which agrees well with the LA value of -8.0 ± 1.3 (2s) (Table 4).

In situ Sm–Nd isotope data for M1439 vesuvianite obtained in three sessions yielded variable $^{147}\text{Sm}/^{144}\text{Nd}$ and $^{143}\text{Nd}/^{144}\text{Nd}$ ratios of 0.1294 ± 0.0269 (2s; $n = 44$) and 0.512264 ± 0.000118 (2s; $n = 44$), respectively (Table 3 and Fig. 4b). The average $^{145}\text{Nd}/^{144}\text{Nd}$ ratio is 0.348380 ± 0.000068 (2s; $n = 44$) (Table 3), which is in agreement with the recommended value.⁶⁶ Solution MC-ICP-MS analysis of one M1439 vesuvianite crystal yielded $^{147}\text{Sm}/^{144}\text{Nd}$ and $^{143}\text{Nd}/^{144}\text{Nd}$ ratios of 0.1255 and 0.512287 ± 0.000023 (2s; $n = 1$), respectively (Table 4). The values obtained by the different methods agree within uncertainties. The $\epsilon_{\text{Nd}}(t)$ value based on the U–Pb age of 158.5 ± 3.1 Ma (2s)¹² is -5.4 ± 0.4 (2s), which is consistent with the LA-based value of -5.9 ± 2.3 (2s) (Table 4).

The calculated $\epsilon_{\text{Nd}}(t)$ values obtained by LA- and solution-based MC-ICP-MS analysis of the three vesuvianite samples

agree well with the wide range of $\epsilon_{\text{Nd}}(t)$ values (-11.5 to -4.2) for the Qianlishan pluton.^{56,57} For mineral deposits, it is useful to utilizing *in situ* analysis of rock-forming minerals in skarn rocks (e.g., vesuvianite) to investigate mechanisms of mineralisation.

5.1.3 Guangxi Province. M1450 vesuvianite has high Sr (1588 ± 616 $\mu\text{g g}^{-1}$) and low Rb (0.14 ± 0.03 $\mu\text{g g}^{-1}$) contents (Table S1†). However, this sample is characterised by low contents of Nd (5.3 ± 11.4 $\mu\text{g g}^{-1}$; Table S1†) and is not suitable for *in situ* Sm–Nd isotope analyses. The chondrite-normalised REE pattern exhibits a large positive Eu anomaly (Fig. 2d), similar to FR vesuvianite from the Furong Sn deposit in the Nanling Range, southern China.¹⁴ Three LA-MC-ICP-MS sessions yielded $^{87}\text{Sr}/^{86}\text{Sr} = 0.70815 \pm 0.00005$ (2s; $n = 15$) to 0.70817 ± 0.00009 (2s; $n = 15$), with an average of 0.70816 ± 0.00010 (2s; $n = 44$) (Table 3 and Fig. 3b). These results are relatively homogeneous and agree well with the solution MC-ICP-MS value of 0.708162 ± 0.000014 (2s; $n = 1$; Table 4). The

in situ Sr isotopic compositions of scheelite (0.70277–0.71471) from the skarn-type ores in the Guposhan ore field are variable and in good agreement with the initial $^{87}\text{Sr}/^{86}\text{Sr}$ ratios of the Guposhan granites (0.7066 ± 0.0027), which are both similar to our vesuvianite Sr isotopic compositions.^{58,59}

M6601 has moderate Sr ($198 \pm 70 \mu\text{g g}^{-1}$) and low Rb ($1.0 \pm 3.1 \mu\text{g g}^{-1}$) contents (Table S1†). M6601 vesuvianite was also not analysed for Sm–Nd isotopes by LA-MC-ICP-MS because of its relatively low Nd content ($41 \pm 50 \mu\text{g g}^{-1}$; Table S1†). It has variable Eu/Eu* values (1.1 ± 1.2) and exhibits slight LREE enrichment (Fig. 2b). $^{87}\text{Sr}/^{86}\text{Sr}$ ratios vary from 0.70929 ± 0.00051 (2s; $n = 10$) to 0.70993 ± 0.00072 (2s; $n = 13$), with an average of 0.70962 ± 0.00079 (2s; $n = 34$) (Table 3 and Fig. 3c). Solution MC-ICP-MS analysis yielded $^{87}\text{Sr}/^{86}\text{Sr} = 0.709796 \pm 0.000014$ (2s; $n = 1$; Table 4). M6601 vesuvianite exhibits large variations in LA-based $^{87}\text{Sr}/^{86}\text{Sr}$ data, despite the close agreement between the LA- and solution-based MC-ICP-MS analyses. Furthermore, some M6601 vesuvianite grains may have high Rb/Sr ratios, which are particularly susceptible to inaccurate isobaric interference corrections.

5.2 Myanmar

Trace element contents of 13MDL176 vesuvianite obtained by LA-ICP-MS exhibit large variations, and moderate Nd ($249 \pm 247 \mu\text{g g}^{-1}$) and Sm ($32 \pm 28 \mu\text{g g}^{-1}$) contents (Table S1†). Because of the relatively low Sr content ($33 \pm 20 \mu\text{g g}^{-1}$; Table S1†), the Sr isotopic composition was not determined by LA-MC-ICP-MS. The chondrite-normalised REE pattern (Fig. 2b) exhibits enrichment in LREEs and LREE/HREE fractionation. The LA-MC-ICP-MS Sm–Nd isotopic data for 13MDL176 vesuvianite obtained in three sessions are presented in Table 3. The $^{147}\text{Sm}/^{144}\text{Nd}$ values exhibit large variations from 0.0848 ± 0.0223 (2s; $n = 15$) to 0.0916 ± 0.0515 (2s; $n = 15$), with an average of 0.0873 ± 0.0358 (2s; $n = 45$), whereas the $^{143}\text{Nd}/^{144}\text{Nd}$ ratios exhibit limited variation from 0.511735 ± 0.000099 (2s; $n = 15$) to 0.511775 ± 0.000076 (2s; $n = 15$), with an average of 0.511756 ± 0.000083 (2s; $n = 45$) (Table 3 and Fig. 4c). The $^{145}\text{Nd}/^{144}\text{Nd}$ ratio of 0.348392 ± 0.000044 (2s; $n = 45$) is consistent with the recommended value of 0.348415 (Table 3).⁶⁶ For the solution MC-ICP-MS analysis, one chip derived from the crystal of 13MDL176 vesuvianite yielded $^{147}\text{Sm}/^{144}\text{Nd} = 0.0938$ and $^{143}\text{Nd}/^{144}\text{Nd} = 0.511777 \pm 0.000014$ (2s; $n = 1$; Table 4). Based on the U–Pb age of 13MDL176 vesuvianite (33.7 ± 2.9 Ma; our unpublished data), the corresponding $\epsilon_{\text{Nd}}(t)$ value for 13MDL176 vesuvianite is -16.4 ± 0.3 (2s), which is within uncertainty of the LA-based value of -16.7 ± 1.6 (2s) (Table 4).

5.3 Russia

The Wilui vesuvianite has moderate Sr ($151 \pm 29 \mu\text{g g}^{-1}$) and low Rb ($0.14 \pm 0.06 \mu\text{g g}^{-1}$) contents (Table S1†). The sample has a relatively low Nd content ($48 \pm 77 \mu\text{g g}^{-1}$; Table S1†), which makes it unsuitable for *in situ* Sm–Nd isotope analysis. The chondrite-normalised REE pattern (Fig. 2d) exhibits strong LREE enrichment and a large positive Eu anomaly. During two LA-MC-ICP-MS sessions, the $^{87}\text{Sr}/^{86}\text{Sr}$ ratios of the Wilui vesuvianite varied from 0.70875 ± 0.00021 (2s; $n = 20$) to 0.70905 ± 0.00060

(2s; $n = 15$), with an average of 0.70888 ± 0.00052 (2s; $n = 35$) (Table 3 and Fig. 3d), which is consistent with the solution MC-ICP-MS value of 0.708724 ± 0.000019 (2s; $n = 4$; Table 4). The Wilui vesuvianite appears to have a relatively large $^{87}\text{Sr}/^{86}\text{Sr}$ range.

The Palaeozoic limestones of the Siberian platform have $^{87}\text{Sr}/^{86}\text{Sr} = 0.7090$ – 0.7095 ,⁶³ and these values are higher than our vesuvianite Sr isotopic compositions. The *in situ* Sr isotopic characteristics of vesuvianite sample Wilui can be interpreted in terms of two-component mixing between limestone and hydrous fluids derived from magmas.^{62,68}

5.4 Czech Republic

Hazlov Vesuvianite has moderate Sr ($486 \pm 82 \mu\text{g g}^{-1}$) and low Rb ($0.17 \pm 0.06 \mu\text{g g}^{-1}$) contents (Table S1†). Hazlov vesuvianite is not suitable for *in situ* Sm–Nd isotope analyses by LA-MC-ICP-MS because of its relatively low Nd content ($64 \pm 72 \mu\text{g g}^{-1}$; Table S1†). The Hazlov vesuvianite is LREE enriched (Fig. 2c) and has a small negative Eu anomaly. During three analytical sessions, LA-MC-ICP-MS analyses of Hazlov vesuvianite yielded $^{87}\text{Sr}/^{86}\text{Sr}$ ratios of 0.70901 ± 0.00036 (2s; $n = 15$) to 0.70925 ± 0.00039 (2s; $n = 15$), with an average of 0.70912 ± 0.00046 (2s; $n = 46$) (Table 3 and Fig. 3e). One chip derived by crushing a crystal of Hazlov vesuvianite was selected for solution MC-ICP-MS analysis and yielded $^{87}\text{Sr}/^{86}\text{Sr} = 0.709177 \pm 0.000014$ (2s; $n = 1$; Table 4). Although this value is in good agreement with the LA-MC-ICP-MS results, this sample is relatively heterogeneous in terms of its Sr isotopic composition. The solution- and LA-based results for our vesuvianite sample Hazlov agree within uncertainties with the values for the Central Bohemian Pluton granitoids (0.7051–0.7129).⁶⁴

5.5 USA

Trace element data of the sample Goodall are reported in Table S1.† Goodall vesuvianite has moderate Sr ($129 \pm 32 \mu\text{g g}^{-1}$) and low Rb ($0.15 \pm 0.07 \mu\text{g g}^{-1}$) contents. However, the sample has a relatively low Nd content ($19 \pm 14 \mu\text{g g}^{-1}$; Table S1†), which renders it unsuitable for Sm–Nd isotopic measurements. The chondrite-normalised REE pattern (Fig. 2d) exhibits enrichment in LREEs and a small positive Eu anomaly, like the FR vesuvianite.¹⁴ *In situ* Sr isotope measurements yielded large variations during two analytical sessions, with $^{87}\text{Sr}/^{86}\text{Sr}$ ratios of 0.70945 ± 0.00032 (2s; $n = 16$) to 0.71018 ± 0.00040 (2s; $n = 15$) and an average of 0.70980 ± 0.00082 (2s; $n = 31$) (Table 3 and Fig. 3f). Our solution MC-ICP-MS analysis yielded $^{87}\text{Sr}/^{86}\text{Sr} = 0.710196 \pm 0.000018$ (2s; $n = 1$; Table 4), which is within uncertainty of the LA values.

6. Discussion

6.1 Potential for *in situ* Sr isotope analysis of vesuvianite

There are three prerequisites for accurate and precise *in situ* Sr isotope analyses: high Sr contents, low Rb/Sr ratios, and low Er/Sr or Yb/Sr ratios. Therefore, not all vesuvianite samples have the potential to be analysed for their Sr isotopic compositions *via in situ* LA techniques. Vesuvianite has a wide range of Sr contents (~ 20 to $\sim 4600 \mu\text{g g}^{-1}$) and low Rb contents ($< 1 \mu\text{g g}^{-1}$)

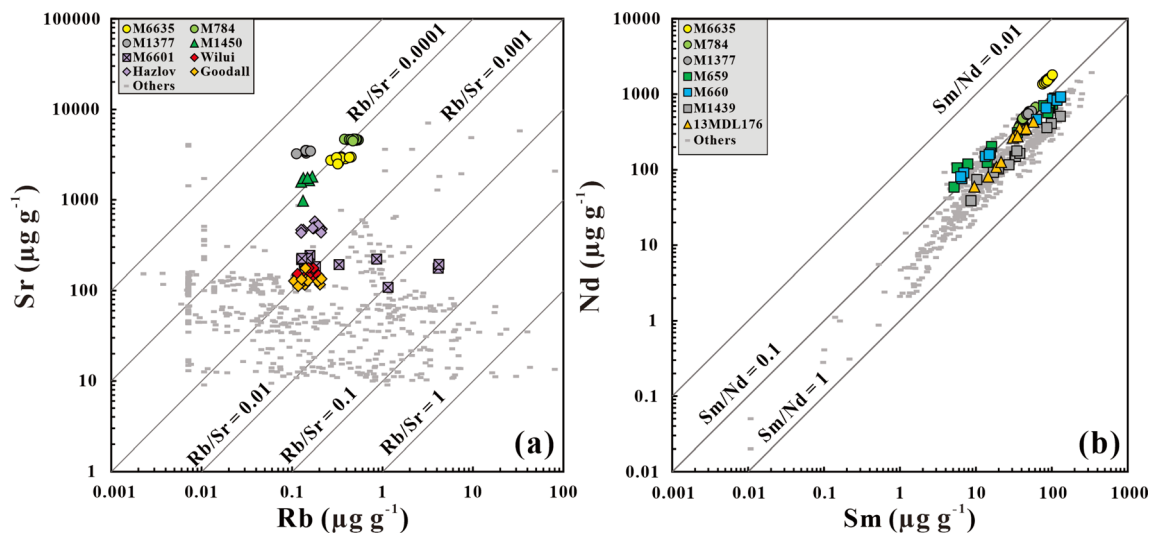


Fig. 5 Plots of (a) Rb–Sr and (b) Sm–Nd for the vesuvianite samples, including data from Halama *et al.*,⁶ Fukuyama *et al.*,⁷ Guo *et al.*,⁸ Caucia *et al.*,⁹ Xing *et al.*,¹³ Zhang *et al.*,¹⁴ Ma *et al.*,²¹ Su *et al.*,⁷⁴ Xu *et al.*,⁷⁵ and He *et al.*⁷⁶

(Table S1[†]). Previous studies have demonstrated that $\sim 500 \mu\text{g g}^{-1}$ Sr is sufficient to acquire a high precision of ± 0.0001 for $^{87}\text{Sr}/^{86}\text{Sr}$ ratios using a laser spot size of 100–160 μm .^{72,73} For vesuvianite samples with moderate Sr contents (~ 100 to $\sim 500 \mu\text{g g}^{-1}$; e.g., vesuvianite samples M6601, Wilui, Hazlov, and Goodall), similar to Xu *et al.*,³⁷ the jet sample and X skimmer cones coupled with the addition of 4 mL min^{-1} N_2 were used to enhance the signal intensity and achieve high precision. A low Rb/Sr ratio is also required for *in situ* Sr isotope analyses because of the interference of ^{87}Rb on ^{87}Sr . In most cases, data for samples with $\text{Rb}/\text{Sr} < 0.02$ ($^{87}\text{Rb}/^{86}\text{Sr} < 0.05$) can be accurately corrected.^{15,73} The investigated vesuvianite samples have $\text{Rb}/\text{Sr} = 0.00003\text{--}0.02$, and M6601 vesuvianite has large variations of Rb/Sr ratios between 0.0005 and 0.02 (Fig. 5a). For some

vesuvianite samples, like M6601, it is necessary to carry out detailed trace element analysis before *in situ* Sr isotope measurements in order to avoid sample grains with high Rb/Sr ratios. Finally, vesuvianite typically has high REE contents due to the REE substituting for Ca^{2+} . Yang *et al.*¹⁶ showed that Er/Sr or Yb/Sr ratios should be < 0.1 to obtain accurate and precise *in situ* Sr isotopic data. As shown in Fig. 6a, the investigated vesuvianite samples have Er/Sr and Yb/Sr ratios of 0.0003–0.04 and 0.0002–0.05, respectively, which indicate the interference of doubly charged ions on ^{84}Sr and ^{86}Sr can be accurately corrected.

No well-characterised, matrix-matched, reference materials are available for *in situ* Sr isotope analysis of vesuvianite. To assess the reliability of our methods, an in-house vesuvianite

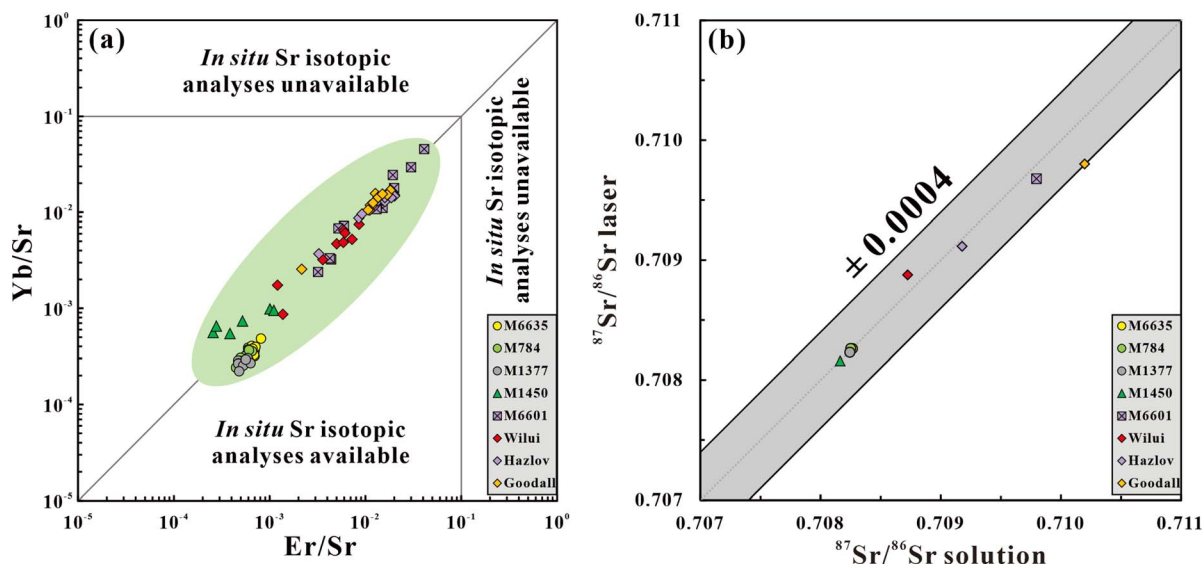


Fig. 6 (a) Er/Sr and Yb/Sr variations showing the possible compositional ranges required to obtain accurate Sr isotope data for vesuvianite using the LA-MC-ICP-MS method. (b) Plots of $^{87}\text{Sr}/^{86}\text{Sr}$ (solution) versus $^{87}\text{Sr}/^{86}\text{Sr}$ (laser ablation) for the studied vesuvianite samples.

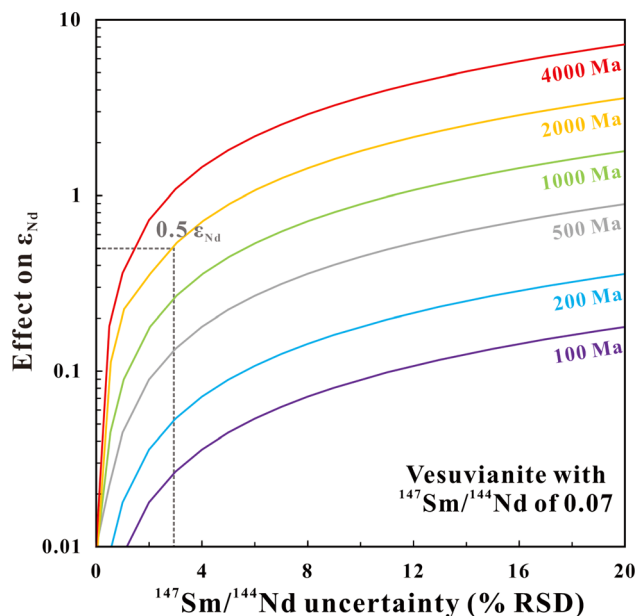


Fig. 7 Effects on the $\epsilon_{\text{Nd}}(0)$ values of radiogenic in-growth of ^{143}Nd in vesuvianite (variable crystallisation ages; $^{147}\text{Sm}/^{144}\text{Nd} = 0.07$). For a ca. 2 Ga vesuvianite sample, the $^{147}\text{Sm}/^{144}\text{Nd}$ uncertainty has to be $<3\%$ to obtain an uncertainty of $<0.5\epsilon_{\text{Nd}}$ on the $\epsilon_{\text{Nd}}(0)$ value.

standard (M6635) was analysed using solution and LA methods. The M6635 vesuvianite has a homogeneous Sr isotopic composition and was used to externally calibrate the other data during this study. After the corrections, the $^{87}\text{Sr}/^{86}\text{Sr}$ ratios calculated from the LA data are consistent with those obtained from the solution analyses (Fig. 6b), with a precision of ± 0.0004 for the $^{87}\text{Sr}/^{86}\text{Sr}$ ratios, which demonstrates the accuracy of the Sr isotope data for the vesuvianite samples obtained by LA-MC-

ICP-MS. The sample-standard bracketing method for *in situ* Sr isotope analysis is often used to correct for possible instrumental mass-independent fractionation effects,^{31,32} wherein the matrix effect between the sample and standard is negligible. In this study, we did not evaluate the matrix effect on the *in situ* Sr isotope analysis of vesuvianite.

6.2 Potential for *in situ* Sm–Nd isotope analysis of vesuvianite

The Sm/Nd ratio is a key variable for initial Nd isotopic measurements. Considering that our investigated vesuvianite samples have Sm/Nd ratios of 0.05–0.25 (<1 ; Fig. 5b), all samples could be precisely measured by LA-MC-ICP-MS analysis.^{27,29} The accuracy of the $^{147}\text{Sm}/^{144}\text{Nd}$ measurement is also important, especially when working with ancient samples.^{27,30,77} The potential ϵ_{Nd} deviation with respect to the uncertainty of the vesuvianite $^{147}\text{Sm}/^{144}\text{Nd}$ ratio of 0.07 is shown in Fig. 7. For a ca. 2 Ga vesuvianite sample, the $^{147}\text{Sm}/^{144}\text{Nd}$ uncertainty must be $<3\%$ to obtain an uncertainty of $<0.5\epsilon_{\text{Nd}}$ on the initial ϵ_{Nd} value. In this case, the $^{147}\text{Sm}/^{144}\text{Nd}$ uncertainty has less effect on the initial ϵ_{Nd} values because of the relatively low $^{147}\text{Sm}/^{144}\text{Nd}$ ratios of vesuvianite.

There is no suitable vesuvianite standard for *in situ* Sm–Nd isotopic measurements. The primary vesuvianite standard used in this study is M659. Its $^{147}\text{Sm}/^{144}\text{Nd}$ values exhibit relatively minor variations (RSD $\sim 9.5\%$), and the Nd isotopic composition is homogeneous (Table 3). Previous studies have suggested that non-matrix-matched corrections can result in systematic bias of Sm–Nd isotope data (between 2% to 5%).^{16,78} Therefore, we evaluated the matrix effect on the *in situ* Sm–Nd isotope analysis of vesuvianite and glass, using M659 vesuvianite and NIST SRM 610 glass as the external standards. As shown in Fig. 8, although the vesuvianite data corrected with M659 vesuvianite and NIST SRM 610 glass are within $\pm 1\epsilon_{\text{Nd}}$, the former is relatively closer to the values obtained

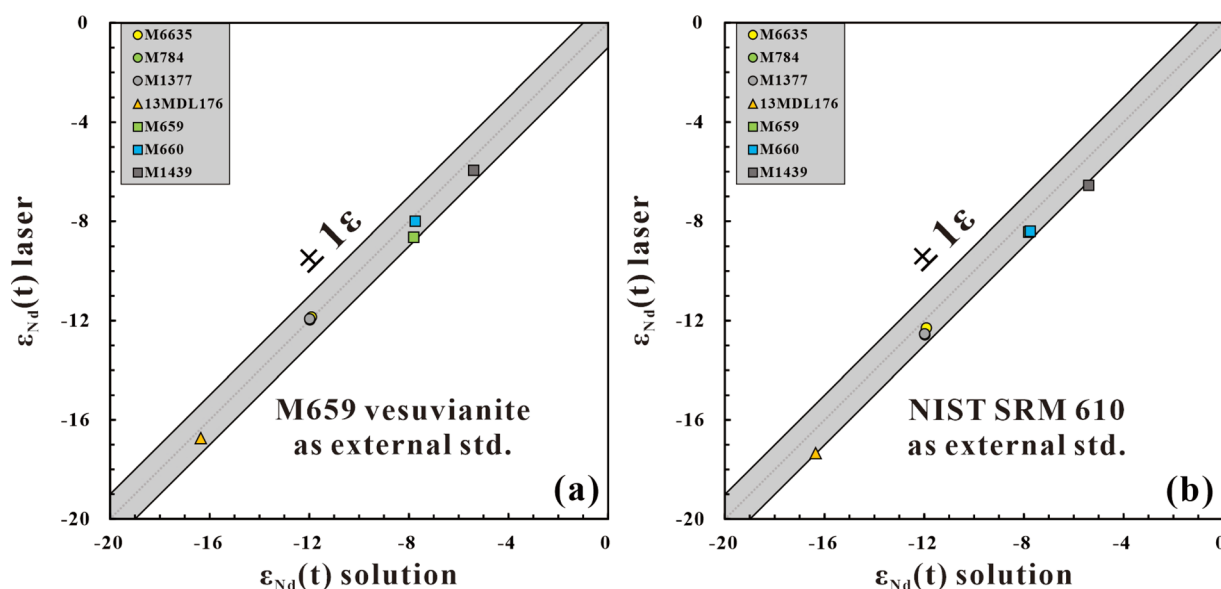


Fig. 8 Plots of $\epsilon_{\text{Nd}}(t)$ (solution) versus $\epsilon_{\text{Nd}}(t)$ (laser ablation) for the studied vesuvianite samples. (a) M659 vesuvianite was used as an external standard for the other vesuvianite samples. (b) NIST SRM 610 was used as an external standard.

using the solution-based method. These results mean that natural mineral standards with homogeneous Sm–Nd isotopic compositions are preferable for *in situ* Sm–Nd isotope studies, especially for minerals with high $^{147}\text{Sm}/^{144}\text{Nd}$.^{18,38,48}

6.3 Potential reference materials for *in situ* Sr and Sm–Nd isotope analyses of vesuvianite

There are several key features of ideal reference materials for *in situ* vesuvianite Sr and Sm–Nd isotope analysis. First, in all cases, Sr or Nd isotopic compositions should be homogenous on both micro and bulk scales. Moreover, ideal reference materials for vesuvianite should also display minor variations of $^{147}\text{Sm}/^{144}\text{Nd}$ values. Second, the ideal standard should contain enough Sr or Nd to obtain precise and accurate data. In addition, with regard to *in situ* Sr isotope analyses, Rb/Sr, Er/Sr, and Yb/Sr ratios must be below the recommended values so that the isobaric interferences can be corrected. For *in situ* Sm–Nd isotope analyses, a known crystallisation age is also indispensable for calculation of the initial Nd isotope ratio. Finally, the reference materials should have a practically unlimited supply to the scientific community for routine use.^{15,16,18–20,78}

M6635, M784, M1377, and M1450 vesuvianites have high Sr ($>1000 \mu\text{g g}^{-1}$) and low Rb ($<0.5 \mu\text{g g}^{-1}$) contents and relatively homogeneous $^{87}\text{Sr}/^{86}\text{Sr}$ ratios ($2s < 0.0001$), indicating they are potential vesuvianite reference materials for *in situ* Sr isotope analyses. Another four vesuvianite samples (M6601, Wilui, Hazlov, and Goodall) that have moderate Sr contents and a relatively large range of $^{87}\text{Sr}/^{86}\text{Sr}$ ratios are not suitable as Sr isotope reference materials. The *in situ* $^{147}\text{Sm}/^{144}\text{Nd}$ values of M659 vesuvianite have the lowest relative standard deviation (RSD $\sim 9.5\%$) among all the vesuvianite samples, and the sample has relatively homogeneous $^{143}\text{Nd}/^{144}\text{Nd}$ ratios ($2s: \sim 0.00005$). Therefore, M659 vesuvianite is suitable as a reference material for *in situ* Sm–Nd isotopic measurements. Vesuvianite samples M6635 and M784, which have homogeneous initial $^{143}\text{Nd}/^{144}\text{Nd}$ ratios, are not suitable as reference materials because of their variable $^{147}\text{Sm}/^{144}\text{Nd}$ ratios with RSD values of $>14\%$ and $>26\%$, respectively, but appropriate to quality control during the analyses.

7. Conclusions

Strontium and Sm–Nd isotope analyses of vesuvianite have the potential to provide important information regarding petrogenesis of alkaline magmas, skarn or contact metasomatic systems. We established an analytical protocol for *in situ* Sr–Nd isotope analyses of vesuvianite by LA-MC-ICP-MS. We carried out both LA- and solution-based measurements of the Sr or Nd isotopic compositions of 12 vesuvianite samples. Our LA-MC-ICP-MS Sr and Nd isotopic compositions for these vesuvianite samples are all consistent with the values obtained by solution-based methods (MC-ICP-MS), demonstrating the feasibility and reliability of *in situ* Sr and Sm–Nd isotope analysis. We recommend that M6635, M784, M1377, and M1450 vesuvianite are suitable as reference materials for *in situ* Sr isotope analyses,

and M659 vesuvianite is a potential reference material for *in situ* Sm–Nd isotope analyses.

Author contributions

Qin-Di Wei: conceptualization, formal analysis, investigation, methodology, visualization, writing – original draft. Yue-Heng Yang: conceptualization, formal analysis, funding acquisition, methodology, writing – review & editing. Hao Wang: supervision, project administration, writing – review & editing. Shi-Tou Wu: formal analysis, validation. Ming Yang: formal analysis, funding acquisition, writing – review & editing. Chao Huang: software, validation. Lei Xu: formal analysis, validation. Lie-Wen Xie: formal analysis, validation. Jin-Hui Yang: supervision, project administration. Fu-Yuan Wu: supervision, project administration.

Conflicts of interest

There are no conflicts to declare.

Acknowledgements

This study was financed by the National Key R&D Program of China (2018YFA0702600), the National Natural Science Foundation of China (No. 42303025), and the State Key Laboratory of Lithospheric Evolution, Institute of Geology and Geophysics, Chinese Academy of Sciences (SKL-Z202304). We are indebted to Prof. Shun Guo for providing vesuvianite sample 13MDL176. If readers are interested in our in-house Microsoft Excel macros, we would be delighted to share them.

References

- 1 G. R. Himmelberg and T. P. Miller, *Am. Mineral.*, 1980, **65**, 1020–1025.
- 2 L. A. Groat, F. C. Hawthorne and T. S. Ercit, *Can. Mineral.*, 1992, **30**, 19–48.
- 3 R. Bogoch, S. Kumarapeli and A. Matthews, *Can. Mineral.*, 1997, **35**, 1269–1275.
- 4 S. Fitzgerald, P. B. Leavens, A. L. Rheingold and J. A. Nelen, *Am. Mineral.*, 1987, **72**, 625–628.
- 5 T. T. Nyunt, T. Theye and H. J. Massonne, *Period. Mineral.*, 2009, **78**, 5–18.
- 6 R. Halama, I. P. Savov, D. Garbe-Schoenberg, V. Schenk and T. Toulkeridis, *Eur. J. Mineral.*, 2013, **25**, 193–219.
- 7 M. Fukuyama, M. Ogasawara, H. Sato, D. Ishiyama and T. Nishiyama, *Can. Mineral.*, 2012, **50**, 1373–1386.
- 8 S. Guo, Y. Chen, C. Z. Liu, J. G. Wang, B. Su, Y. J. Gao, F. Y. Wu, S. Kyaing, Y. H. Yang and Q. Mao, *J. Asian Earth Sci.*, 2016, **117**, 82–106.
- 9 F. P. Caucia, L. Marinoni, M. Scacchetti, M. P. Riccardi and O. Bartoli, *Minerals*, 2020, **10**, 535.
- 10 E. Gnos and T. Armbruster, *Am. Mineral.*, 2006, **91**, 862–870.
- 11 R. L. Romer, *Mineral. Petrol.*, 1992, **46**, 331–341.

- 12 Q. D. Wei, M. Yang, R. L. Romer, H. Wang, Y. H. Yang, Z. F. Zhao, S. T. Wu, L. W. Xie, C. Huang, L. Xu, J. H. Yang and F. Y. Wu, *J. Anal. At. Spectrom.*, 2022, **37**, 69–81.
- 13 L. Z. Xing, J. T. Peng, Y. J. Lv, Y. W. Tang and J. F. Gao, *Chem. Geol.*, 2022, **607**, 121017.
- 14 Y. Zhang, S. L. Song, P. Hollings, D. F. Li, Y. J. Shao, H. Y. Chen, L. J. Zhao, S. Kamo, T. T. Jin, L. L. Yuan, Q. Q. Liu and S. C. Chen, *Chem. Geol.*, 2022, **612**, 121136.
- 15 Y. H. Yang, F. Y. Wu, S. A. Wilde, X. M. Liu, Y. B. Zhang, L. W. Xie and J. H. Yang, *Chem. Geol.*, 2009, **264**, 24–42.
- 16 Y. H. Yang, F. Y. Wu, J. H. Yang, D. M. Chew, L. W. Xie, Z. Y. Chu, Y. B. Zhang and C. Huang, *Chem. Geol.*, 2014, **385**, 35–55.
- 17 T. Iizuka, S. M. Eggins, M. T. McCulloch, L. P. J. Kinsley and G. E. Mortimer, *Chem. Geol.*, 2011, **282**, 45–57.
- 18 Q. Ma, N. J. Evans, X. X. Ling, J. H. Yang, F. Y. Wu, Z. D. Zhao and Y. H. Yang, *Geostand. Geoanal. Res.*, 2019, **43**, 355–384.
- 19 Y. H. Yang, F. Y. Wu, Q. L. Li, Y. Rojas-Agramonte, J. H. Yang, Y. Li, Q. Ma, L. W. Xie, C. Huang, H. R. Fan, Z. F. Zhao and C. Xu, *Geostand. Geoanal. Res.*, 2019, **43**, 543–565.
- 20 M. Yang, Y. H. Yang, S. L. Kamo, R. L. Romer, N. M. W. Roberts, H. Wang, L. W. Xie, C. Huang, J. H. Yang and F. Y. Wu, *Geostand. Geoanal. Res.*, 2022, **46**, 169–203.
- 21 L. Y. Ma, Y. F. Lu, J. M. Fu, X. Q. Chen and S. B. Cheng, *South China Geol.*, 2010, **4**, 23–29, (in Chinese with English abstract).
- 22 H. A. Gilg, A. Lima, R. Somma, H. E. Belkin, B. De Vivo and R. A. Ayuso, *Mineral. Petrol.*, 2001, **73**, 145–176.
- 23 J. P. Davidson, D. J. Morgan, B. L. A. Charlier, R. Harlou and J. M. Hora, *Annu. Rev. Earth Planet. Sci.*, 2007, **30**, 273–311.
- 24 J. Gillespie, A. A. Nemchin, P. D. Kinny, L. Martin, M. Aleshin, M. P. Roberts, T. R. Ireland, M. J. Whitehouse, H. Jeon, A. J. Cavosie and C. L. Kirkland, *Chem. Geol.*, 2021, **559**, 119979.
- 25 J. Hammerli, A. I. S. Kemp and C. Spandler, *Earth Planet. Sci. Lett.*, 2014, **392**, 133–142.
- 26 J. F. Sun, J. H. Zhang, J. H. Yang, Y. H. Yang and S. Chen, *Lithos*, 2019, **334**, 42–57.
- 27 G. L. Foster and D. Vance, *J. Anal. At. Spectrom.*, 2006, **21**, 288–296.
- 28 C. R. M. McFarlane and M. T. McCulloch, *Chem. Geol.*, 2007, **245**, 45–60.
- 29 Y. H. Yang, J. F. Sun, L. W. Xie, H. R. Fan and F. Y. Wu, *Chin. Sci. Bull.*, 2008, **53**, 1062–1070, (in Chinese with English abstract).
- 30 C. M. Fisher, C. R. M. McFarlane, J. M. Hanchar, M. D. Schmitz, P. J. Sylvester, R. Lam and H. P. Longerich, *Chem. Geol.*, 2011, **284**, 1–20.
- 31 L. Yang, Z. Mester, L. Zhou, S. Gao, R. E. Sturgeon and J. Meija, *Anal. Chem.*, 2011, **83**, 8999–9004.
- 32 R. Xu, Y. S. Liu, X. R. Tong, Z. C. Hu, K. Q. Zong and S. Gao, *Chem. Geol.*, 2013, **354**, 107–123.
- 33 K. P. Jochum, U. Weis, B. Stoll, D. Kuzmin, Q. C. Yang, I. Raczek, D. E. Jacob, A. Stracke, K. Birbaum, D. A. Frick, D. Günther and J. Enzweiler, *Geostand. Geoanal. Res.*, 2011, **35**, 397–429.
- 34 S. T. Wu, G. Wörner, K. P. Jochum, B. Stoll, K. Simon and A. Kronz, *Geostand. Geoanal. Res.*, 2019, **43**, 567–584.
- 35 S. T. Wu, Y. H. Yang, N. M. W. Roberts, M. Yang, H. Wang, Z. W. Lan, T. Y. Li, L. Xu, C. Huang, L. W. Xie, J. H. Yang and F. Y. Wu, *Sci. China Earth Sci.*, 2022, **64**, 187–190.
- 36 W. L. Griffin, W. J. Powell, N. J. Pearson and S. Y. O'Reilly, *Short Course Ser. – Mineral. Assoc. Can.*, 2008, **40**, 308–311.
- 37 L. Xu, Z. C. Hu, W. Zhang, L. Yang, Y. S. Liu, S. Gao, T. Luo and S. H. Hu, *J. Anal. At. Spectrom.*, 2015, **30**, 232–244.
- 38 Y. H. Yang, Z. Y. Chu, S. T. Wu, L. W. Xie, C. Huang, J. H. Yang and F. Y. Wu, *At. Spectrosc.*, 2023, **44**, 247–252.
- 39 K. P. Jochum and B. Stoll, *Mineral. Assoc. Can.*, 2008, 147–168.
- 40 F. C. Ramos, J. A. Wolff and D. L. Tollstrup, *Chem. Geol.*, 2004, **211**, 135–158.
- 41 H. Zhao, X. M. Zhao, P. J. Le Roux, W. Zhang, H. Wang, L. W. Xie, C. Huang, S. T. Wu, J. H. Yang, F. Y. Wu and Y. H. Yang, *Front. Chem.*, 2020, **8**, 594316.
- 42 J. N. Christensen, A. N. Halliday, D. C. Lee and C. M. Hall, *Earth Planet. Sci. Lett.*, 1995, **136**, 79–85.
- 43 M. Bizzarro, A. Simonetti, R. K. Stevenson and S. Kurszlaukis, *Geochim. Cosmochim. Acta*, 2003, **67**, 289–302.
- 44 J. Woodhead and J. Hergt, *Geostand. Geoanal. Res.*, 2005, **29**, 183–195.
- 45 R. K. O'Nions, P. J. Hamilton and N. M. Evensen, *Earth Planet. Sci. Lett.*, 1977, **34**, 13–22.
- 46 J. C. Dubois, G. Retali and J. Cesario, *Int. J. Mass Spectrom. Ion Processes*, 1992, **120**, 163–177.
- 47 H. Isnard, R. Brennetot, C. Caussignac, N. Caussignac and F. Chartier, *Int. J. Mass Spectrom.*, 2005, **246**, 66–73.
- 48 Y. H. Yang, F. Y. Wu, Z. Y. Chu, L. W. Xie and J. H. Yang, *Spectrochim. Acta Part B At. Spectrosc.*, 2013, **79–80**, 82–87.
- 49 J. Lin, Y. S. Liu, Y. H. Yang and Z. C. Hu, *Solid Earth Sci.*, 2016, **1**, 5–27.
- 50 Y. H. Yang, H. F. Zhang, Z. Y. Chu, L. W. Xie and F. Y. Wu, *Int. J. Mass Spectrom.*, 2010, **290**, 120–126.
- 51 Y. H. Yang, Z. Y. Chu, F. Y. Wu, L. W. Xie and J. H. Yang, *J. Anal. At. Spectrom.*, 2011, **26**, 1237–1244.
- 52 Y. H. Yang, F. Y. Wu, Z. C. Liu, Z. Y. Chu, L. W. Xie and J. H. Yang, *J. Anal. At. Spectrom.*, 2012, **27**, 516–522.
- 53 A. Fourny, D. Weis and J. S. Scoates, *Geochem. Geophys. Geosyst.*, 2016, **17**, 739–773.
- 54 Y. S. Zhu, J. H. Yang, J. F. Sun, J. H. Zhang and F. Y. Wu, *J. Asian Earth Sci.*, 2016, **117**, 184–207.
- 55 P. L. Zhao, S. D. Yuan, J. W. Mao, Y. B. Yuan, H. J. Zhao, D. L. Zhang and Y. Shuang, *Ore Geol. Rev.*, 2018, **95**, 1140–1160.
- 56 Y. X. Chen, H. Li, W. D. Sun, T. Ireland, X. F. Tian, Y. B. Hu, W. B. Yang, C. Chen and D. R. Xu, *Lithos*, 2016, **266**, 435–452.
- 57 C. L. Guo, R. C. Wang, S. D. Yuan, S. H. Wu and B. Yin, *Mineral. Petrol.*, 2015, **209**, 253–282.
- 58 Y. S. Gu, R. M. Hua and H. W. Qi, *Acta Geol. Sin.*, 2006, **80**, 543–553, (in Chinese with English abstract).
- 59 J. Y. Cao, H. Li, T. J. Algeo, L. Z. Yang and L. S. Tamehe, *Am. Mineral.*, 2021, **106**, 1488–1502.

- 60 M. P. Searle, S. R. Noble, J. M. Cottle, D. J. Waters, A. H. G. Mitchell, T. Hlaing and M. S. A. Horstwood, *Tectonics*, 2007, **26**, TC3014.
- 61 N. J. Gardiner, M. P. Searle, L. J. Robb and C. K. Morley, *J. Asian Earth Sci.*, 2015, **106**, 197–215.
- 62 I. Galuskina, E. Galuskin and M. Sitarz, *Neues Jahrb. Mineral. Monatsh.*, 1998, **2**, 49–62.
- 63 S. V. Alexeev, L. P. Alexeeva, V. N. Borisov, O. Shouakar-Stash, S. K. Frape, F. Chabaux and A. M. Kononov, *Russ. Geol. Geophys.*, 2007, **48**, 225–236.
- 64 V. Janoušek, G. Rogers and D. R. Bowes, *Geol. Rundsch.*, 1995, **84**, 520–534.
- 65 D. L. Leavitt and N. J. Leavitt, *Mineral. Rec.*, 1993, **24**, 359–364.
- 66 G. J. Wasserburg, S. B. Jacobsen, D. J. DePaolo, M. T. McCulloch and T. Wen, *Geochim. Cosmochim. Acta*, 1981, **45**, 2311–2323.
- 67 W. F. McDonough and S. S. Sun, *Chem. Geol.*, 1995, **120**, 223–253.
- 68 I. Galuskina, E. Galuskin and M. Sitarz, *Neues Jahrb. Mineral. Monatsh.*, 2001, **2**, 49–66.
- 69 G. W. Lugmair and K. Marti, *Earth Planet. Sci. Lett.*, 1978, **39**, 349–357.
- 70 S. B. Jacobsen and G. J. Wasserburg, *Earth Planet. Sci. Lett.*, 1980, **50**, 139–155.
- 71 S. L. Goldstein, R. K. Onions and P. J. Hamilton, *Earth Planet. Sci. Lett.*, 1984, **70**, 221–236.
- 72 Y. H. Yang, F. Y. Wu, L. W. Xie, J. H. Yang and Y. B. Zhang, *Acta Petrol. Sin.*, 2009, **25**, 3431–3441, (in Chinese with English abstract).
- 73 F. Y. Wu, Y. H. Yang, M. A. W. Marks, Z. C. Liu, Q. Zhou, W. C. Ge, J. S. Yang, Z. F. Zhao, R. H. Mitchell and G. Markl, *Chem. Geol.*, 2010, **273**, 8–34.
- 74 H. Su, X. J. Wang, Z. M. Chen and S. Z. Li, *Acta Mineral. Sin.*, 2016, **36**, 529–534, (in Chinese with English abstract).
- 75 J. Xu, C. L. Ciobanu, N. J. Cook, Y. Zheng, X. Sun and B. P. Wade, *Lithos*, 2016, **262**, 213–231.
- 76 C. T. He, K. Z. Qin, J. X. Li, Q. F. Zhou, J. X. Zhao and G. M. Li, *Acta Petrol. Sin.*, 2020, **36**, 3593–3606.
- 77 C. M. Fisher, A. M. Bauer, Y. Luo, C. Sarkar, J. M. Hanchar, J. D. Vervoort, S. R. Tapster, M. Horstwood and D. G. Pearson, *Chem. Geol.*, 2020, **539**, 119493.
- 78 Z. C. Liu, F. Y. Wu, Y. H. Yang, J. H. Yang and S. A. Wilde, *Chem. Geol.*, 2012, **334**, 221–239.